UNIVERSIDAD NACIONAL AUTÓNOMA DE MÉXICO

PROGRAMA DE MAESTRÍA Y DOCTORADO EN INGENIERÍA

INSTITUTO DE INGENIERÍA

FORMULATION AND APPROXIMATION TO PROBLEMS IN SOLIDS BY EMBEDDED DISCONTINUITY MODELS

T E S I S

PARA OBTENER EL GRADO DE:

DOCTOR EN INGENIERÍA

INGENIERÍA CIVIL – ESTRUCTURAS

PRESENTA:

JAIME RETAMA VELASCO

DIRECTOR DE TESIS:

DR. A. GUSTAVO AYALA MILIÁN

CIUDAD UNIVERSITARIA, MÉXICO, D.F.,
SEPTIEMBRE, 2010

**INSTITUTO
DE INGENIERÍA**
UNAM

Contents

List of Figures

Abstract

The simulation of the problem of damage undergone by a solid, by means of numerical and computational models, is a topic of interest in different areas of science whose complexity has led to the development of numerical methods to simulate the material degradation under various load conditions, which may eventually lead to the failure of the solid.

In this context, different numerical models which consider the damage as a degradation of the material properties, without redefining the kinematics of the continuum, have been developed. The *smeared cracking* and *continuum damage* formulations belong to this type of models. Other formulations like the *Extended Finite Element Method*, XFEM, and the *Partition of Unity* model simulate the damage by modifying the materials properties, and the kinematics of the continuum by introducing an enhancement in the relevant field variables, which bear the required discontinuity only where it appears.

Strictly speaking the above formulations smear the damage into the entire element, using a finite element approximation; however this type of models do not properly simulate the damage process where a localized crack occurs, characteristic of damage in quasi–brittle materials, leading to an unloading of the bulk. This type of problems can only be correctly modeled by means of formulations which introduce the damage as a geometrical discontinuity, using cohesive material models. Formulations as the *embedded discontinuity model* belong to this type which use an enhancement of the kinematics at elemental level.

In this work, the damage problem in solids is carried out by means of the embedded discontinuity formulation, in its discrete approach, introducing a cohesive crack inside the element domain. Two constitutive laws are used, one linear elastic for the bulk, and the other a cohesive, *traction–jump*, for the discontinuity boundary. Rigid body motion of the parts in which the element is divided is assumed.

Since the embedded discontinuity formulation, presented in this work, is consistently derived from the general canonical variational formulation of *De Veubeke–Hu–Washizu*, valid for a continuum solid; it satisfies all the field equations of the associated *boundary value problem*, complemented by equations which state the traction equilibrium across the crack, also derived in a natural way from the variational formulation.

Following a *finite element* discretization of the domain, two different formulations are developed: a displacement where the only independent field is the displacement and a mixed formulation with the displacement and strain fields as independent. Unlike the standard finite element formulation where the displacement field is continuous; in these

finite element formulations, commonly known as *finite elements with discontinuities*, the interpolated fields may be discontinuous to allow that the crack crosses the element. In this work only linear constant strain triangular elements are used.

Although the variational formulation satisfies all the field equations and the equilibrium of tractions across the crack, in natural form, the use of a numerical method to approximate the solution of the problem leads to an imposition of these conditions in *weak* form. In this research a new variable is introduced to enforce the traction equilibrium in *strong* form at elemental level. It is shown that the response is dependent on the crack geometry; unlike the non–symmetric formulation, when the crack continuity is not enforce across elements, which is invariant with respect to this. Therefore, enforcement of the traction equilibrium in *strong* form is directly related with the crack localization inside the element, which defines its geometry.

For the numerical implementations of the developed formulations, the *Finite Element Analysis Program* (FEAP), is used. Since the enhancement of the relevant fields are introduced only at elemental level, an *static condensation* is performed to eliminate the additional degrees of freedom, related with enhanced deformation modes; preserving only those used in the standard formulation of the finite element method, displacements.

To validate the numerical and theoretical consistency of the presented embedded discontinuity formulations, two numerical examples are presented at the end of the work. In these problems the damage is simulated by considering only the Mode–I of failure, for quasi–brittle materials, since no shear stresses are allowed along the crack. The numerical simulation results are compared with those reported from experimental tests. Special emphasis in given to the global response of the solid in the process of energy dissipation across the crack.

Resumen

El problema de la simulación numérica y computacional del daño experimentado por un sólido, es un tema de interés en diversas áreas de la ciencia cuya complejidad ha dado lugar al desarrollo de nuevos modelos numéricos que permiten simular el proceso de degradación de los materiales ante diversas condiciones de carga, que eventualmente llevan al sólido al colapso.

En este contexto, se tienen modelos numéricos que consideran el problema de daño como una degradación de las propiedades mecánicas del material sin la necesidad de redefinir la cinemática del continuo; este tipo de modelos incluyen el de *agrietamiento distribuido* y el de *daño continuo*. En esta misma dirección se encuentran los modelos donde, además de modificar la ley constitutiva del material de acuerdo al daño que éste experimenta, modifican la cinemática del continuo al enriquecer los campos en los que se requiere un comportamiento discontinuo; modelos como el del *elemento finito extendido*, XFEM por sus siglas en ingles, y el de *partición de la unidad* pertenecen a este tipo de modelos numéricos.

Estrictamente hablando los modelos anteriormente mencionados, en su aproximación mediante el método de los elementos finitos, distribuyen el daño en todo el elemento; sin embargo ésto no permite modelar correctamente grietas localizadas o procesos de daño en materiales donde claramente existe una discontinuidad que provoca una descarga de las partes en las que el sólido se divide. Para simular este tipo de problemas de daño, se han desarrollado modelos, como el de discontinuidades interiores que situan el daño, en consistencia con el problema físico, mediante una discontinuidad física dentro del elemento; ésto se logra al enriquecer el campo de desplazamientos y/o de deformaciones.

En esta tesis se estudia el problema del daño en sólidos mediante la formulación de discontinuidades interiores en su aproximación discreta; donde el daño se introduce como una grieta cohesiva dentro del elemento y su comportamiento constitutivo está caracterizado por modelos cohesivos *tracción–salto*. El efecto del salto sobre el comportamiento del continuo se refleja por un mevimiento de cuerpo rígido de las parte en que el sólido se divide; experimentando una descarga elástica lineal.

La formulación de discontinuidades interiores, presentada en este trabajo, es consistente desde el punto de vista energético. Su formulación variacional se deriva a partir de la formulación canónica de *De Veubeke–Hu–Washizu* para un sólido continuo, dentro de la teoría de la elasticidad. El funcional para un sólido con discontinuidades considera la

energía disipada en las grietas, durante el proceso de daño. Se demuestra que la formulación variacional satisface todas las ecuaciones de campo que gobiernan el problema de valores en la frontera; complementadas por las ecuaciones que establecen la continuidad de tracciones a través de la grieta, derivadas de forma natural.

Para la aproximación de los campos se utiliza el *método del elemento finito* en sus formulaciones de: desplazamientos y mixta de desplazamientos–deformaciones. La cinamática de desplazamientos y de deformaciones utilizada, permiten que la grieta cruce el elemento al utilizar funciones de interpolación discontinuas en aquellos campos donde se require un comportamiento discontinuo de éstos. Ésto da lugar a elementos finitos no estándares que se les conoce como *elementos finitos con discontinuidades*. Los elementos desarrollados en este trabajo son elementos triangulares lineales de deformación constante.

A pesar de que la formulación variacional satisface el equilibrio de tracciones de manera natural, al aproximar su solución mediante el método del elemento finito se presenta el problema de que esta condición no se impone apropiadamente. Para satisfacer el equilibrio, en este trabajo se introduce una nueva variable en la formulación con la que se logra imponer de manera fuerte el equilibrio de tracciones a través de la grieta, a nivel elemental. Se demuestra que la ubicación de la grieta dentro del elemento influye en el resultado numérico; sin embargo, solamente existe una ubicación en la que el aquilibrio se impone correctamente. Ésto muestra que la localización de la grieta es una variable en la formulación de discontinuidades interiores presentada en este trabajo.

Las formulaciones desarrolladas se implementan numéricamente en el programa de elementos finitos FEAP (acrónimo de su nombre en idioma Inglés, *Finite Element Analysis Program*); utilizando la *condensación estática* para eliminar los grados de libertad elementales y únicamente preservando los grados de libertad de desplazamiento asociados a la formulación estándar del método del elemento finito.

Para validar la consistencia numérica y teórica de las fomulaciones desarrolladas, al final del trabajo se presentan dos ejemplos de aplicación en los que se simula el proceso del daño que experimenta el sólido hasta alcanzar la falla total, considerando el Modo–I de falla para materiales cuasi–frágiles. Los resultados obtenidos se comparan con los reportados de los ensayes de laboratorio; particularmente la respuesta global del continuo en el proceso de disipación de la energía a través de la grieta.

Chapter 1

Introduction

The numerical simulation of the growth of cracks in damaged solids has posed a scientific challenge for decades. Two main paths can be distinguished: the modeling of fracture in a smeared sense, within a continuum theory, and the modeling of fracture in a discrete sense, [92, 110].

The basic mathematical theory, for the study of fracture in a solid, was given in the classical paper of Inglis in 1913, [52], who obtained the elastic solution for stresses at the vertex of an ellipsoidal cavity in an infinite solid and observed that, as the ellipse approached a line crack, the stresses at the vertex of the ellipse become unbounded, figure 1.1. This basic result became the foundation of the *Linear Elastic Fracture Mechanics* (LEFM), [6, 14, 24, 82].

Today LEFM is a basic tool for the analysis of many structural problems dealing with crack growth. However, it is applicable only when the material is brittle, which means that the material remains elastic up to the initiation of fracture, *i.e.,* the fracture process zone has to be small compared with the relevant dimensions of the specimen. Furthermore, LEFM lacks a detailed description of what is happening in the fracture process zone because it lumps all the inelastic effects into the crack tip.
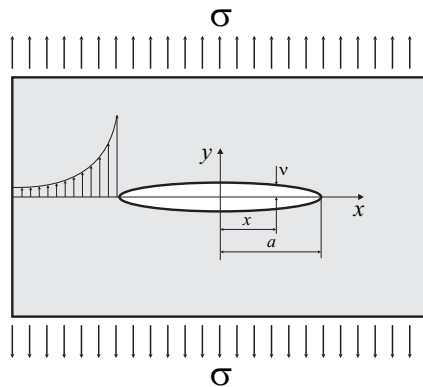
Figure 1.1: Variation of stresses at the crack tip as the ellipse tends to a line.
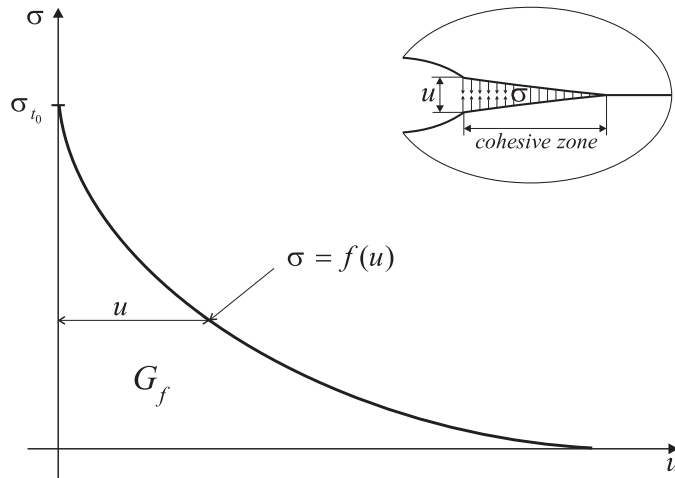
Figure 1.2: Stress *versus* displacement curve and the cohesive process zone.

The way in which the fracture process is modeled in the LEFM, within a finite element approximation, leads to consider that cracks occur on the boundaries of the elements since, standard finite elements are employed. This implies that a crack should exists and the mesh has to be modified continuously to accommodate its orientation parallel to the elements boundaries.

The need of remeshing, associated with the propagation of the crack in the LEFM, involves an excessive computational cost because at each loading step, the mesh has to be modified. Moreover, the use of standard finite elements (displacement formulation), leads to the use of a method to smooth the stress field like the proposed by Zienkiewicz and Zhu [119].

An alternative, to study the problem of fracture in solids, emerges from classical continuum mechanics. These models appeared in 1960's decade when, with the support of numerical methods such as the *Finite Element Method* (FEM) [16, 51, 85, 117] , a more effective description of the fracture phenomenon was given. Within the FEM context, two different types of models may be distinguished: one in which the inelastic deformations of the fracture process zone is smeared over a band of a certain width and the other in which the entire fracture process is lumped into a crack line which behavior is characterized by a stress–displacement law known as cohesive zone models [14, 49, 106, 110].

1.1 Discrete modeling of fracture

An important issue when considering failure is the observation that most engineering materials are not perfectly brittle in the Griffith sense. In fact there exists a small zone in front of a crack tip, in which micro–cracking and void initiation, growth and coalescence take place. If this fracture process zone is sufficiently small compared with the smallest structural dimension, LEFM concepts can be applied, however, if this is not the case, the cohesive forces that exist in this zone must be taken into account. The natural way,

2

to consider cohesive forces across a crack, is to use *cohesive zone models*, introduced by Barenblatt [15] and Dugdale [36] for elastic–plastic fracture in ductile metals, and for quasi–brittle materials by Hillerborg *et al.,* [49] in his so–called fictitious crack model.

For the fictitious crack model, the degrading mechanisms are lumped into a discrete line or plane, figure 1.2, and a stress–displacement relationship across this line is used to simulate the progressive degradation of the material in this zone [67]. In figure 1.2 it may be seen that this degradation phenomenon begins once the maximum principal stress reaches the tensile strength σ_{to} of the material.

For brittle materials, considering a Ranking failure criterion, the most important parameters of the cohesive zone model appear to be the tensile strength, σ_{to}, and the work involved in the separation of the crack or fracture energy, G_f, [21] which is the work needed to create a fully developed crack of unit area [6, 14],

$$ G_F = \int_0^u \sigma \, \mathrm{d}u \tag{1.1} $$

where σ is a characteristic stress defined on the surface and u is the displacement, both defined in figure 1.2.

The other form in which the cohesive forces across the discontinuity can be taken into account in the constitutive model, is by smearing the degradation of the material properties in a band of width different from zero where inelastic effects are developed.

1.2 Continuum modeling of fracture

Development of damage in a material is mainly the process of the initiation and growth of micro–cracks and cavities, figure 1.3. Kachanov was the first in 1958, to introduce a continuum variable related to the density of such defects, [14, 61, 65, 66, 112]. Since this pioneer work, there has been a great development in the continuum damage mechanics models.

Generally, the failure process in a material is an irreversible phenomenon, during which the entropy increases. Kachanov proposed to consider the variable damage d as a surface density of intersections of cracks and cavities in the material.

However, even some results obtained using these finite element models, are very promising; the numerical results of this kind of models with strain softening are strongly dependent on the size of the elements of the mesh [14, 93]. To overcome this difficulty, some authors have implemented models where one additional material parameter, absent in the classical theory, is required [13, 44, 45, 57]. All these models employ a length scale which controls the width of the process zone in which strains localize.
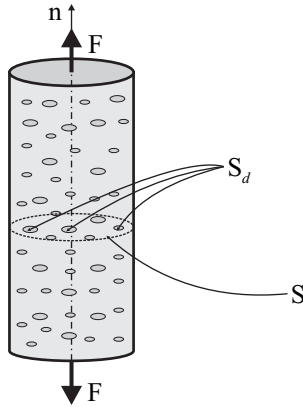
Figure 1.3: One dimensional damaged element.

1.3   The embedded discontinuity approach

Recently, a different approach in which a crack crosses the element, figure 1.4, has been developed. This approach emerged as a mean to deal with general strain localization phenomena (such as shear bands in metals) of which the cohesive crack is a particular case (Belytschko *et al.,* [18], Simo and Rifai [102], Dvorkin [37], Simo *et al.,* [101], Lotfi and Shing [69], Oliver [78], Larsson and Runesson [64], Alfaiate *et al.,* [4], Júarez and Ayala [60]).

All embedded discontinuities approaches have a common basic underlying, the process zone is incorporated into the variational formulation of a finite element model by an enhancement in the interpolation of the relevant fields [86, 90], which bears the required discontinuity only where it appears, so that the model of the main field is not affected by the enhancement. This form of considering discontinuous fields, eliminates the continuous remeshing process inherent in the classic LEFM model.

In the framework of the embedded discontinuity formulation, three different approaches may be identified attending to their constitutive models employed and the kinematics of displacement and strain fields used [41, 59].
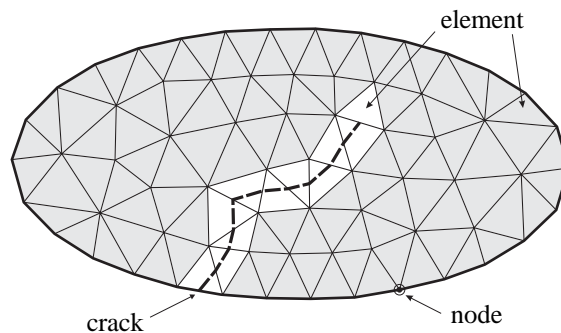
Figure 1.4: Solid with an internal crack discretized by the FEM.
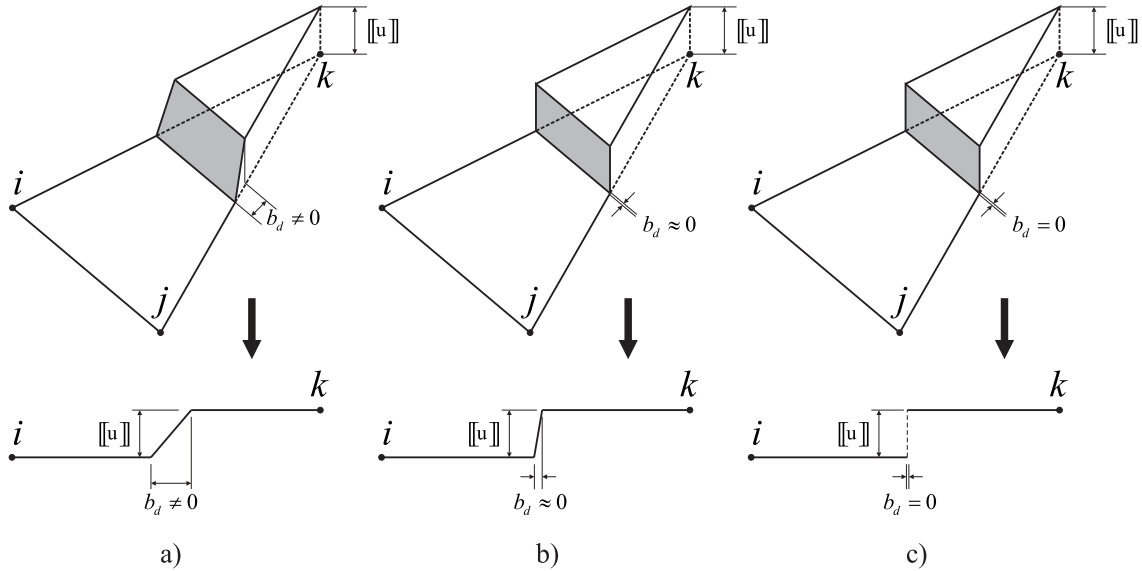
Figure 1.5: Embedded discontinuity models.

1.3.1 Continuum approach

This approach considers the solid as a continuum in all its domain and the behavior of the material is modeled by standard strain–stress constitutive laws. The *weak* and *strong* embedded discontinuity formulations belong to this kind of models.

1. *Weak discontinuity.* In this formulation the displacement field is continuous and the strain field is discontinuous. The process zone is located into a bandwidth different from zero, figure 1.5a.

2. *Strong discontinuity.* This formulation is obtained from the *weak* discontinuity approach when the strain localization zone tends to zero, leading to a discontinuous displacement field and an unbounded strain field across the discontinuity, figure 1.5b.

1.3.2 Discrete approach

The main difference of this approach with the *strong* approach is that in here two constitutive laws are used; one strain–stress relationship for the bulk and other a traction–jump relationship for the discontinuity boundary. Strictly speaking, in these models the solid becomes a discrete body where tractions are applied on the discontinuity boundary, figure 1.5c.

In the present work the discrete embedded discontinuity approach will be employed according to the variational formulation developed by Júarez and Ayala [59, 60] and that presented by Alfaiate in [1].

5

1.4 Outline of the thesis

In what follows, a general description of the thesis contents is given.

- Chapter 2. The kinematics involving the displacement and strain fields, of the discrete discontinuity approach, is developed in consistency with the finite element method. The kinematics of displacements and strains, for a one dimensional problem, is established; similar to the *Assumed Enhanced Strain* method. The generalization of these equations to the three dimensional case, is straightforward.

- Chapter 3. To simulate the crack growth a traction–jump constitutive law is employed. The damage is introduced considering cohesive forces across the crack faces; whereas the bulk, materials in the neighborhood of the crack surfaces, unloads elastically. The material model considered is based on an isotropic formulation where the evolution of the crack is modeled according to the Mode–I of fracture.

- Chapter 4. In this chapter the most general variational formulation for a solid without discontinuities is reviewed. It is shown that this variational formulation satisfies all the field equations of the associated *Boundary Value Problem* together with the essential and natural boundary conditions. A hierarchy of variational formulations is recovered when it is assumed that some equations are *a priori* satisfied.

- Chapter 5. The energy dissipation in a discontinuity surface is taken into account, in the development of the variational formulation for a solid with discontinuities. It is shown that, in addition to the *Boundary Value Problem* equations, the continuity of tractions across the crack surface is obtained in a natural form. In section 5.2, an approximation of the field equations by the FEM is used together with the kinematics equations derived in chapter 2. A general description of the non–symmetric embedded discontinuity formulation is given at the of this chapter.

- Chapter 6. Despite the fact that in the variational formulation the traction continuity is correctly satisfied; when a numerical method is used to approximate the solution of the differential equations system, it is shown that the equilibrium at the discontinuity is satisfied in strong form only on a particular surface; introducing a new variable in the formulation.

- Chapter 7. Since in the presented formulation the additional enhanced deformation modes are considered as elemental ones, in its numerical implementation it is possible to eliminated these additional degrees of freedom to preserve only those as for the standard FEM. The numerical implementation is carried out in the *Finite Element Analysis Program* (FEAP).

- Chapter 8. To validate the mathematical consistency of the developed embedded discontinuity formulation, two different numerical examples are presented. The first example is an uniaxial tension test, and the second example is the classical four

points beam with a single notched; originally used to study the influence of a mixed failure mode, tension and shear, in the global behavior of quasi–brittle materials. For both examples only the Mode–I of failure is considered together with two softening laws, linear and exponential.

- Capter 9. General comments and conclusions, relative to the presented symmetric embedded discontinuity formulation, are given in chapter 9.

Chapter 2

Kinematics of the discontinuity

In this chapter the kinematics of the displacement and strain fields of a solid crossed by a discontinuity is analyzed.

Consider a body with domain Ω and boundary Γ, figure 2.1, where essential boundary conditions, $\bar{\mathbf{u}}$, exist on Γ_u and natural boundary conditions, $\bar{\mathbf{t}}$, are applied on Γ_t, such that $\Gamma = \Gamma_u \cup \Gamma_t$ and $\emptyset = \Gamma_u \cap \Gamma_t$. Additionally, the body is crossed by a discontinuity Γ_d which divides the domain Ω into two subdomains Ω^+ and Ω^-, $\Omega = \Omega^- \cup \Omega^+$. On the discontinuity boundary, the normal $\mathbf{n}$ is defined pointing towards Ω^+.

Within the framework of the embedded discontinuity formulation, three different approaches are used. The *weak* and *strong* discontinuity correspond to a continuum approach where strain–stress constitutive laws are used in all the domain Ω, while in the *discrete* two constitutive laws are employed; one strain–stress constitutive law, for the bulk, and one traction–jump relationship, on the discontinuity Γ_d. A *weak* discontinuity is characterized by a jump on the strain field across a band of finite width b_d, figure 2.1, where the strain field becomes discontinuous but bounded, whereas the displacement field remains continuous everywhere, [88]. A *strong* discontinuity is characterized by a jump on the displacement field across a surface Γ_d, where strains are unbounded, see figure 2.1. The strong discontinuity approach can be regarded as a limit case of the *weak* discontinuity when the width of the localization band, b_d, tends to zero, collapsing into a localized
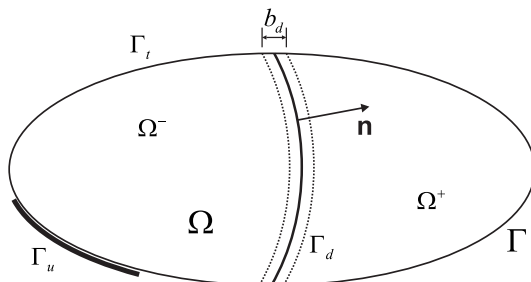
Figure 2.1: Body Ω crossed by a discontinuity Γ_d.

surface Γ_d.

In this work the *discrete* embedded discontinuity approach is adopted. For this approach, when the strength of the material is reached, the deformation due to micro–cracking or other inelastic phenomena suddenly localizes at a discontinuous surface Γ_d.

2.1 Displacement jump

The displacement field $\mathbf{u}$ for a body, crossed by a discontinuity, figure 2.1 can be decomposed into a continuous and discontinuous part [4, 78, 116],

$$\mathbf{u}(\mathbf{x}, t) = \hat{\mathbf{u}}(\mathbf{x}, t) + \mathcal{H}_{\Gamma_d}(\mathbf{x}) \, [\![\mathbf{u}]\!](\mathbf{x}, t) \tag{2.1}$$

where $\hat{\mathbf{u}}$ and $[\![\mathbf{u}]\!]$ are smooth, continuous functions on Ω and $\mathcal{H}_{\Gamma_d}$ is the Heaviside function centered at the discontinuity and defined as,

$$\mathcal{H}_{\Gamma_d} = \begin{cases} \alpha_d & \forall \, \mathbf{x} \in \Omega^+ \\ 1 - \alpha_d & \forall \, \mathbf{x} \in \Omega^- \end{cases} \tag{2.2}$$

where α_d is a constant which defines how the jump is transmitted, $0 \le \alpha_d \le 1$; if $\alpha_d = 0$ the jump is totally transmitted to Ω^- and if $\alpha_d = 1$ the jump is transmitted to Ω^+.

The corresponding infinitesimal strain field, for a body crossed by a discontinuity, can be found by taking the symmetric gradient of equation (2.1)

$$\boldsymbol{\varepsilon} = \boldsymbol{\nabla}^s \hat{\mathbf{u}} + \mathcal{H}_{\Gamma_d}(\boldsymbol{\nabla}^s [\![\mathbf{u}]\!]) + (\boldsymbol{\nabla}\mathcal{H}_{\Gamma_d} \otimes [\![\mathbf{u}]\!])^s = \underbrace{\hat{\boldsymbol{\varepsilon}}}_{bounded} + \underbrace{\delta_{\Gamma_d}([\![\mathbf{u}]\!] \otimes \mathbf{n})^s}_{unbounded} \tag{2.3}$$

where δ_{Γ_d} is the Dirac–delta distribution centered at the discontinuity Γ_d, satisfying,

$$\int_\Omega \delta_{\Gamma_d} \, \phi \mathrm{d}\Omega = \int_{\Gamma_d} \phi \, \mathrm{d}\Gamma \tag{2.4}$$

The strain field, given by equation (2.3), can be decomposed into a bounded part $\hat{\boldsymbol{\varepsilon}}$ plus an unbounded, irregular part, given by $\delta_{\Gamma_d}([\![\mathbf{u}]\!] \otimes \mathbf{n})^s$. The unbounded part of the strain field can be taken into account in two different ways: i) regularizing the Dirac–delta by means of a bandwidth parameter close to zero $b_d \approx 0$, [64, 78, 79], or ii) no regularization is considered, taking advantage of the properties of the Dirac–delta function, equation (2.4), [8, 114, 116].

10
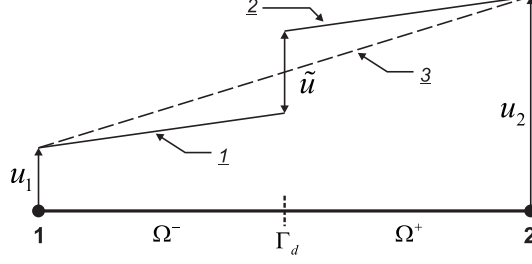
Figure 2.2: One dimensional finite element with a discontinuity.

2.2 Finite element approximation

In section 2.1 a general form of the discontinuity kinematic has been given; now a consistent interpolation functions will be derived. The displacement and strain fields will be constructed only from kinematic considerations like in [37, 69].

Consider a one dimensional finite element crossed by the discontinuity Γ_d, as it is shown in figure 2.2. It is assumed that Ω^+ undergoes a rigid body incremental displacement $\tilde{u}$ with respect to Ω^-. In order to obtain the same incremental displacement derivatives on both subdomains, the interpolations represented in figure 2.2 by lines 1 and 2 may be adopted for Ω^- and Ω^+ respectively. Their mathematical expressions are:

$$u_1 = \mathbf{N}\left[\mathbf{u} - \begin{pmatrix} 0 \\ 1 \end{pmatrix}\tilde{u}\right] \tag{2.5}$$

for the left subdomain Ω^- and

$$u_2 = \mathbf{N}\left[\mathbf{u} - \begin{pmatrix} 0 \\ 1 \end{pmatrix}\tilde{u}\right] + \tilde{u} \tag{2.6}$$

for the right subdomain Ω^+. The purpose of matrix $\mathcal{H}_{\Gamma_d} = (0 \ \ 1)^T$ in equations (2.5) and (2.6) can be understood from the analysis of figure 2.2. As expected, for every point either in Ω^- or Ω^+ the infinitesimal strain is

$$\boldsymbol{\varepsilon} = \boldsymbol{\nabla}^s\mathbf{u} = \mathbf{B}\left[\mathbf{u} - \begin{pmatrix} 0 \\ 1 \end{pmatrix}\tilde{u}\right] = \mathbf{B}(\mathbf{u} - \mathcal{H}_{\Gamma_d}\tilde{u}) \tag{2.7}$$

where $\mathbf{B}$ is the usual strain–displacement transformation matrix, [16, 85, 117], and matrix $\mathcal{H}_{\Gamma_d}$ is given by equation (2.2).

For a two–dimensional case, these concepts can be properly generalized by introducing the vector $[\![\mathbf{u}]\!]$ containing the components of the displacement jumps associated with the discontinuity Γ_d,

$$\llbracket \mathbf{u} \rrbracket = \begin{bmatrix} \tilde{u} \\ \tilde{v} \end{bmatrix} \tag{2.8}$$

Matrix $\mathcal{H}_{\Gamma_d}$, given by equation (2.2), follows from a straightforward generalization of its counterpart in equations (2.5) and (2.6). For a two–dimensional problem, $\mathcal{H}_{\Gamma_d}$ can be rewritten in the general form

$$\boldsymbol{\mathcal{H}}_{\Gamma_d} = \begin{bmatrix} \mathcal{H}^1_{\Gamma_d} \\ \vdots \\ \mathcal{H}^n_{\Gamma_d} \end{bmatrix} \tag{2.9}$$

where n is the number of nodes in the finite element, and each of the submatrices $\mathcal{H}^i_{\Gamma_d}$ depends of the position of node i relative to the discontinuity; hence each of these submatrices may be written as,

$$\mathcal{H}^i_{\Gamma_d} = \begin{cases} \alpha_d \, \mathbf{I} & \forall \, \mathbf{x} \in \Omega^+ \\ (1 - \alpha_d) \, \mathbf{I} & \forall \, \mathbf{x} \in \Omega^- \end{cases} \tag{2.10}$$

where $\mathbf{I}$ is the identity matrix of dimension $(n_{st} \times n_{st})$; and n_{st} is the space dimension of the problem.

From equations (2.5) and (2.6) a displacement function for the whole domain Ω is defined by

$$\mathbf{u} = \mathbf{N}\hat{\mathbf{u}} + (\mathcal{H}_{\Gamma_d} - \mathbf{N}\mathcal{H}_{\Gamma_d})\llbracket \mathbf{u} \rrbracket \tag{2.11}$$

Taking $\mathbf{N}_c$ as

$$\mathbf{N}_c = \mathcal{H}_{\Gamma_d} - \mathbf{N}_u \mathcal{H}_{\Gamma_d} \tag{2.12}$$

Equation (2.11) is written in the following final form,

$$\mathbf{u} = \mathbf{N}\hat{\mathbf{u}} + \mathbf{N}_c \llbracket \mathbf{u} \rrbracket \tag{2.13}$$

By means of this definition of the displacement field, (2.13), the strain kinematics is derived in a consistent form as

$$\boldsymbol{\varepsilon} = \mathbf{B}\hat{\mathbf{u}} + \mathbf{B}_c[\![\mathbf{u}]\!] \tag{2.14}$$

where matrix $\mathbf{B}_c$, is derived by applying the strain–displacement operator to equation (2.12),

$$\mathbf{B}_c = \boldsymbol{\nabla}^s \mathbf{N}_c \tag{2.15}$$

Equations (2.13) and (2.14), define the displacement and strain fields corresponding to the discrete approach of the embedded discontinuity formulation, [1, 59, 69].

For a constant strain triangle and considering a uniform deformation field along the internal interface, figure 2.3, equation (2.15) in rewritten in the following form,

$$\mathbf{B}_c = -\boldsymbol{\nabla}^s \boldsymbol{\varphi}(\mathbf{x}) \tag{2.16}$$

where $\boldsymbol{\varphi}(\mathbf{x})$ contains the shape functions corresponding to nodes in Ω^+, [1, 79, 114], defined as,

$$\boldsymbol{\varphi}(\mathbf{x}) = \sum_{i=1}^{n^+} N_i^+ \tag{2.17}$$

where n^+ denotes the number of nodes belonging to the subdomain Ω^+.
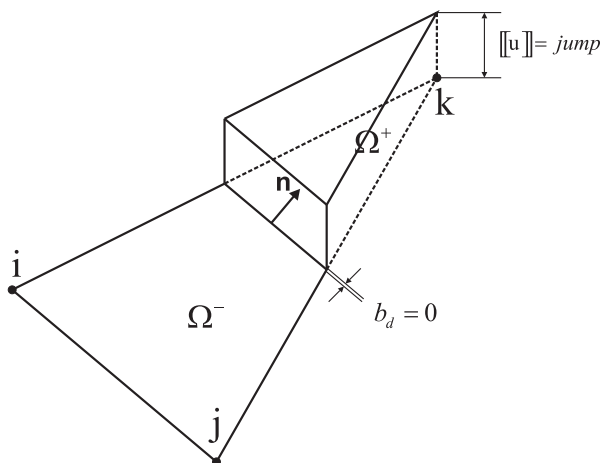
Figure 2.3: Constant strain triangle with a displacement jump.

13

Chapter 3

Discrete damage models

For modeling the evolution of material damage where mode–I type failure is dominant, a cohesive crack type model is used [14, 29, 38, 49, 106]. Micro–cracking and plastic flow around a macroscopic crack tip are modeled as an equivalent traction force on crack faces, figure 3.2. This cohesive crack model was introduced by Barenblatt [15] and Dugdale [36] to represent different nonlinear processes taking place at the tip of a preexisting crack. Since then, cohesive cracks have been extensively used to model crack growth in concrete, ceramics, polymers, and metals, as well as interfaces between different material regions. Specifically Hillerborg [49] extended the work of Barenblatt and Dugdale to simulate cracks growth in concrete by means of finite elements. Since the pioneering work of Hillerborg, many authors have used the concept of *fictitious crack* and *fracture energy G_F* leading to the introduction of true discontinuities [2, 93].

The cohesive approach of Hillerborg, leads to the softening curve shown in figure 3.2 where, $f(w)$ is a function, characteristic of the material, that must be determined from experiments. The function called the *softening curve*, has the property that the limit stress for a zero crack opening is the tensile strength [14, 49], as indicated in the figure.

In this model the inelastic response is governed by two key material parameters: the tensile strength σ_{t_0} and the fracture energy G_F. A discontinuity is introduced when the maximum principal stress exceeds the tensile strength of the material. The normal vector to a discontinuity is aligned in the direction of the maximum principal stress. This mode–I
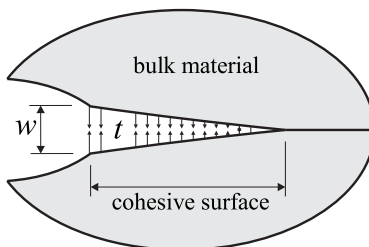
Figure 3.1: Capturing a micro–cracked zone into a cohesive surface.
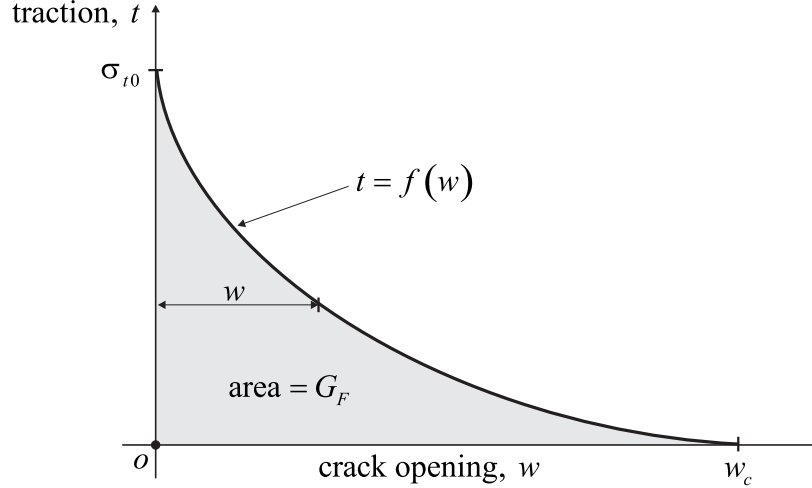
Figure 3.2: Softening curve for a cohesive crack model.

criterion is commonly used for quasi–brittle materials [4, 114, 116].

Since the material around the discontinuity remains elastic, two constitutive models are used to simulate the behavior of the solid. One for the bulk by means of a linear elastic constitutive law, strain–stress relationship, whereas for the fracture zone, where inelastic effects are localized, two different types of discrete damage models may be considered: i) an isotropic damage model and ii) an anisotropic damage model.

A cohesive surface relates the traction $\mathbf{t}$, transmitted over the boundary Γ_d, to the displacements jump $[\![\mathbf{u}]\!]$ between the surfaces, see figure 3.1. In contrast to the continuum damage models in which damage affects the stiffness of a material volume, damage evolution in the cohesive surface model affects the ability to transmit tractions over the cohesive surface. While the bulk of the material remains elastic, the model thus captures anisotropic damage evolution in a natural way since damage develops only on specific surfaces. Fracture of the material now progresses solely based on the strength degradation in the cohesive surfaces and the interaction with the undamaged, elastic, regions of the material.

3.1   Damage model with isotropic softening

A common framework within which many authors deal with damage [4, 42, 65, 70, 106] is, from a thermodynamic point of view, the Helmholtz free energy density Ψ which, in a continuum isotropic model is defined as

$$\Psi(\boldsymbol{\varepsilon}, \omega(r)) = [1 - \omega(r)]\Psi_0(\varepsilon) \tag{3.1}$$

where Ψ_0 is the elastic free energy density dependent on the strain tensor $\boldsymbol{\varepsilon}$, ω is an internal damage variable and r is an internal scalar variable which considers the strain state in the

16

element and is a function of the *fracture energy* G_F. Since in equation (3.1) only isotropic and adiabatic process are considered; ω becomes an scalar parameter representing the state of damage that the continuum experiments. Its value varies from 0, corresponding to an undamaged state, to 1 which represents a fully damaged state. The introduction of this parameter, in the constitutive law, allows the representations of damage evolution.

Similar considerations, as those for continuum damage models, can be made for the formulation of a discrete damage model where a traction–jump relationship is introduced to simulate degradation of the material on the discontinuity boundary and $\psi(\llbracket \mathbf{u} \rrbracket, \omega)$ represents the free energy per unit area [4, 116],

$$\psi \left(\llbracket \mathbf{u} \rrbracket, \omega(\kappa) \right) = [1 - \omega(\kappa)]\psi_0(\llbracket \mathbf{u} \rrbracket) \tag{3.2}$$

where $\llbracket \mathbf{u} \rrbracket$ is the displacement jump vector on the discontinuity boundary Γ_d, κ is an internal scalar variable which can be considered as an equivalent jump ($\kappa = \llbracket u \rrbracket_{eq}$), and ψ_0 is the linear elastic free energy given by

$$\psi_0(\llbracket \mathbf{u} \rrbracket) = \frac{1}{2}\llbracket \mathbf{u} \rrbracket^T \mathbf{T}^{el} \llbracket \mathbf{u} \rrbracket \tag{3.3}$$

where, $\mathbf{T}^{el}$ is the elastic constitutive tensor defined only on the discontinuity boundary Γ_d. Equation (3.3) is valid for a discontinuity with a linear elastic behavior.

For thermal stable problems, the Helmholtz free energy given by equation (3.2) has to satisfy the following inequality of Clausius–Duhem, [46, 65, 100],

$$\mathcal{D} = \mathbf{t}^T \llbracket \dot{\mathbf{u}} \rrbracket - \dot{\psi} \geq 0 \tag{3.4}$$

Equation (3.4) is known as a dissipative potential where, $\mathcal{D}$ is the rate of dissipation energy and $\mathbf{t}$ is the traction vector acting across the discontinuity. A variable with a dot above means its derivative with respect to the time, this is,

$$(\dot{\bullet}) = \frac{\partial}{\partial t}(\bullet) \tag{3.5}$$

Expanding the dissipative potential equation (3.4) according to equation (3.5) and grouping similar terms

$$\mathcal{D} = \left(\mathbf{t} - \frac{\partial \psi}{\partial \llbracket \mathbf{u} \rrbracket} \right)^T \llbracket \dot{\mathbf{u}} \rrbracket + \psi_0 \, \dot{\omega} \geq 0 \tag{3.6}$$

Use of standard thermodynamic arguments, in equation (3.4), leads to the following

17

1. Constitutive equation,

$$\mathbf{t} = \frac{\partial \psi}{\partial [\![\mathbf{u}]\!]} = (1 - \omega)\, \mathbf{T}^{el} [\![\mathbf{u}]\!] \tag{3.7}$$

2. and the dissipation equation is reduced to

$$\mathcal{D} = \psi_0\, \dot{\omega} \geq 0 \tag{3.8}$$

Since the elastic free energy per unit area is positive, $\psi_0 \geq 0$, it can be seen from equation (3.8) that the rate of change of the damage parameter ω cannot be negative, *i.e.,* this parameter can only grow.

3.1.1 Tangent constitutive tensor

Transformation of equation (3.7) into its incremental form by its differentiation with respect to time, leads to the derivation of a tangent constitutive tensor as follows

$$\dot{\mathbf{t}} = (1 - \omega)\mathbf{T}^{el}[\![\dot{\mathbf{u}}]\!] - \dot{\omega}\, \mathbf{T}^{el}[\![\mathbf{u}]\!] = (1 - \omega)\mathbf{T}^{el}[\![\dot{\mathbf{u}}]\!] - \dot{\omega}\, \mathbf{t}^{el} \tag{3.9}$$

where $\mathbf{t}^{el}$ is the elastic traction vector and

$$\dot{\omega} = \frac{d\omega}{d\kappa}\frac{\partial \kappa}{\partial [\![\mathbf{u}]\!]}[\![\dot{\mathbf{u}}]\!] = \frac{d\omega}{d\kappa}\left[\frac{\partial \kappa}{\partial [\![u]\!]_n}[\![\dot{u}]\!]_n + \frac{\partial \kappa}{\partial [\![u]\!]_s}[\![\dot{u}]\!]_s\right] \tag{3.10}$$

Substitution of equation (3.10) into equation (3.9) leads to

$$\dot{\mathbf{t}} = \left[(1 - \omega)\mathbf{T}^{el} - \frac{d\omega}{d\kappa}\mathbf{t}^{el} \otimes \frac{\partial \kappa}{\partial [\![\mathbf{u}]\!]}\right] \cdot [\![\dot{\mathbf{u}}]\!] \tag{3.11}$$

If unloading takes place, the rate of damage is zero, $\dot{\omega} = 0$, and both equations (3.10) and (3.11) reduce to

$$\dot{\mathbf{t}} = (1 - \omega)\mathbf{T}^{el}[\![\dot{\mathbf{u}}]\!] \tag{3.12}$$

3.1.2 Yield function

The development of a discrete damage–type model requires first the definition of a yield function which describes the loading state at a discontinuity surface (loading or unloading/re–loading). The loading function f is given by

$$f = \langle [\![u]\!]_{eq} \rangle - \kappa \leq 0 \tag{3.13}$$

where $[\![u]\!]_{eq}$ is an equivalent jump obtained from the displacement jump $[\![\mathbf{u}]\!]$. The symbols $\langle \cdot \rangle$ are the McAuley brackets denoting that only the positive part of $[\![\mathbf{u}]\!]_{eq}$ is considered in κ.

In equation (3.13), the internal scalar variable κ is a history parameter, equal to the highest value of $\langle [\![u]\!]_{eq} \rangle$ defined as

$$\kappa = \kappa([\![\mathbf{u}]\!]) = max \langle [\![u]\!]_{eq} \rangle \tag{3.14}$$

To complete the description of the model at hand, it is required to determine the slip rate $\dot{\omega} \geq 0$. This involves the following essential conditions that embody the notion of irreversibility inherent in the response of the model.

3.1.3 Loading/unloading conditions

If $f < 0$, the deformation process is reversible and the dissipation rate must be zero, which implies that $\dot{\omega} = 0$. If $f = 0$, the damage can grow such that, in a subsequent state, f remains zero ($\dot{\omega} > 0 \Rightarrow \dot{f} = 0$); both cases can be conveniently expressed by the usual Kuhn–Tucker conditions, [100],

$$\dot{\omega} \geq 0, \quad f \leq 0, \quad \dot{\omega} f = 0, \tag{3.15}$$

together with the consistency condition

$$\dot{\omega} \dot{f} = 0 \tag{3.16}$$

Chapter 4

Variational formulations

Before to the presentation of the functional corresponding to the adopted embedded discontinuity formulation, the energy functional for a solid without discontinuities is established. Consider a continuum body, figure 4.1, with domain Ω, boundary Γ and body forces $\mathbf{b}_v$ applied in Ω. Essential boundary conditions $\bar{\mathbf{u}}$ are defined on Γ_u whereas tractions $\bar{\mathbf{t}}$, corresponding to natural boundary conditions, are applied on Γ_t; such that $\Gamma = \Gamma_u \cup \Gamma_t$ and $\emptyset = \Gamma_u \cap \Gamma_t$. The outward normal vector $\boldsymbol{\nu}$ is defined on Γ_t.

It is possible to show that the energy functional of the general variational principle of *De Veubeke–Hu–Washizu* (VHW) [30, 31, 76, 113], is a generalization of the *Potential Energy* functional for an elastic body. To begin with, the steps by which this functional is derived from the *Principle of Virtual Work* are summarized. It is assumed that: *i*) it is possible to derive a positive definite state function $\Psi(\varepsilon_x, \varepsilon_y, ..., \varepsilon_{xy})$, more briefly denoted by $\Psi(\boldsymbol{\varepsilon})$, hereafter the strain energy density; *ii*) the strain field satisfies the conditions of compatibility, *iii*) the displacement field satisfies the essential boundary conditions defined on Γ_u, and *iv*) body forces and surface tractions can be derived from the potential functions $\Phi(\mathbf{u})$ and $\phi(\mathbf{u})$, functions of the displacement field. The existence of the function $\Psi(\boldsymbol{\varepsilon})$, gives rise to the total strain energy calculated from the integrable field $\boldsymbol{\varepsilon}$,
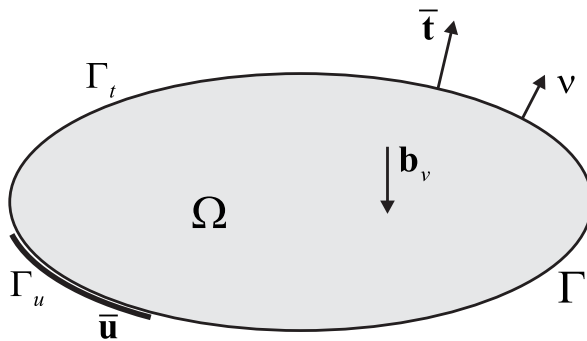
Figure 4.1: Continuous solid with domain Ω and boundary Γ.

$$U = \int_\Omega \Psi(\boldsymbol{\varepsilon}) \, \mathrm{d}\Omega \tag{4.1}$$

Regarding the conditions involved in *ii*) and *iii*), this are introduced through a dislocation potential as

$$D = \int_\Omega \boldsymbol{\sigma}^T (\mathbf{Du} - \boldsymbol{\varepsilon}) \, \mathrm{d}\Omega + \int_{\Gamma_u} \mathbf{t}^T (\bar{\mathbf{u}} - \mathbf{u}) \, \mathrm{d}\Gamma \tag{4.2}$$

where $\boldsymbol{\sigma}$ and $\mathbf{t}$ are the stress and traction fields respectively, and $\mathbf{D}$ is the symmetric gradient operator, defined in appendix B.

The stress and tractions fields may be seen, consistently with mathematical theory, *as Lagrangean multipliers* [31, 40, 113], removing the compatibility conditions *ii*) and *iii*), that must be satisfied *a priori* in the simpler *principle of minimum potential energy*.

The potential energy of prescribed loads is given as

$$P = -\int_\Omega \Phi(\mathbf{u}) \, \mathrm{d}\Omega - \int_{\Gamma_t} \phi(\mathbf{u}) \, \mathrm{d}\Gamma \tag{4.3}$$

where

$$\Phi(\mathbf{u}) = \mathbf{u}^T \mathbf{b}_v \tag{4.4}$$

$$\phi(\mathbf{u}) = \mathbf{u}^T \bar{\mathbf{t}} \tag{4.5}$$

Equations (4.4) and (4.5) are the respective body forces and prescribed tractions, which may be functions of the displacements field $\mathbf{u}$. Hereafter conservative loads are considered, *i.e.,* independent of the loading path in the solid, therefore $\Phi(\mathbf{u}) = \Phi$ and $\phi(\mathbf{u}) = \phi$.

Setting equations (4.1) to (4.5) into a variational formulation, the following generalization of the Principle of Minimum Potential Energy is recovered

$$\delta\Pi(\mathbf{u}, \boldsymbol{\varepsilon}, \boldsymbol{\sigma}, \mathbf{t}) = \delta(U + P + D) = 0 \tag{4.6}$$

where the energy functional Π is written as

$$\Pi = \int_{\Omega} [\boldsymbol{\sigma}^T (\mathbf{Du} - \boldsymbol{\varepsilon}) + \Psi(\boldsymbol{\varepsilon}) - \mathbf{u}^T \mathbf{b}_v] \, d\Omega - \int_{\Gamma_t} \mathbf{u}^T \bar{\mathbf{t}} \, d\Gamma + \int_{\Gamma_u} \mathbf{t}^T (\bar{\mathbf{u}} - \mathbf{u}) \, d\Gamma \qquad (4.7)$$

The functional stated in equation (4.7) considers four independent fields subjected to variations: displacements $\mathbf{u}$, strains $\boldsymbol{\varepsilon}$, stresses $\boldsymbol{\sigma}$ and tractions $\mathbf{t}$; and three dependent fields: strains which depend on the displacement field $\mathbf{u}$, $\mathbf{Du}$, stresses $\boldsymbol{\sigma}(\boldsymbol{\varepsilon})$ dependent on the strain field $\boldsymbol{\varepsilon}$ and stresses $\boldsymbol{\sigma}(\mathbf{u})$ derived from the displacements $\mathbf{u}$.

The strain energy density function $\Psi(\boldsymbol{\varepsilon})$, for a body with elastic behavior, is given as

$$\Psi(\boldsymbol{\varepsilon}) = \int_0^{\boldsymbol{\varepsilon}} (\boldsymbol{\sigma}^{\varepsilon})^T \, d\boldsymbol{\varepsilon} \qquad (4.8)$$

where $\boldsymbol{\sigma}^{\varepsilon} = \boldsymbol{\sigma}(\boldsymbol{\varepsilon})$ are the stresses derived from the independent strain field $\boldsymbol{\varepsilon}$ through a constitutive relationship as $\mathbf{C}\boldsymbol{\varepsilon}$. If in equation (4.8) a constitutive tensor $\mathbf{C}$ for a linear elastic medium is considered, this equation is modified to obtain,

$$\Psi(\boldsymbol{\varepsilon}) = \frac{1}{2}\boldsymbol{\varepsilon}^T \mathbf{C} \boldsymbol{\varepsilon} \qquad (4.9)$$

Taking the first variation of functional (4.7) with respect to each independent field and applying the stationarity conditions (4.6)

$$\delta\Pi = \int_{\Omega} \left[\boldsymbol{\sigma}^T (\mathbf{D}\boldsymbol{\eta}) - \mathbf{b}_v^T \boldsymbol{\eta} \right] d\Omega - \int_{\Gamma_t} \bar{\mathbf{t}}^T \boldsymbol{\eta} \, d\Gamma - \int_{\Gamma_u} \mathbf{t}^T \boldsymbol{\eta} \, d\Gamma +$$
$$\int_{\Omega} \left[\frac{\partial \Psi}{\partial \boldsymbol{\varepsilon}} - \boldsymbol{\sigma} \right]^T \boldsymbol{\gamma} \, d\Omega + \int_{\Omega} [\mathbf{Du} - \boldsymbol{\varepsilon}]^T \boldsymbol{\tau} \, d\Omega + \int_{\Gamma_u} [\bar{\mathbf{u}} - \mathbf{u}]^T \bar{\boldsymbol{\tau}} \, d\Gamma = 0 \qquad (4.10)$$

where $(\boldsymbol{\eta}, \boldsymbol{\gamma}, \boldsymbol{\tau}, \bar{\boldsymbol{\tau}})$ are the variations of displacements, strains, stresses and tractions fields respectively. The integral $\int_{\Omega} \boldsymbol{\sigma}^T (\mathbf{D}\boldsymbol{\eta}) \, d\Omega$ can be rewritten by means of the divergence theorem, appendix B, as

$$\int_{\Omega} \boldsymbol{\sigma}^T (\mathbf{D}\boldsymbol{\eta}) \, d\Omega = - \int_{\Omega} (\boldsymbol{\sigma}^T \mathbf{D}) \boldsymbol{\eta} \, d\Omega + \int_{\Gamma_t} (\boldsymbol{\sigma}^T \mathbf{P}_{\nu}) \boldsymbol{\eta} \, d\Gamma + \int_{\Gamma_u} (\boldsymbol{\sigma}^T \mathbf{P}_{\nu}) \boldsymbol{\eta} \, d\Gamma \qquad (4.11)$$

and $\mathbf{P}_{\nu}$ is the normal–projection matrix, defined as in appendix B, containing the components of the normal vector $\boldsymbol{\nu}$. Substitution of equation (4.11) into (4.10) and grouping similar terms into integrals,

$$\delta\Pi = -\int_{\Omega} \left[\mathbf{D}^T\boldsymbol{\sigma} + \mathbf{b}_v\right]^T \boldsymbol{\eta} \, \mathrm{d}\Omega + \int_{\Omega} \left[\frac{\partial\Psi}{\partial\boldsymbol{\varepsilon}} - \boldsymbol{\sigma}\right]^T \boldsymbol{\gamma} \, \mathrm{d}\Omega + \int_{\Omega} [\mathbf{Du} - \boldsymbol{\varepsilon}]^T \boldsymbol{\tau} \, \mathrm{d}\Omega$$

$$+ \int_{\Gamma_t} \left[\boldsymbol{\sigma}^T\mathbf{P}_\nu - \bar{\mathbf{t}}\right]^T \boldsymbol{\eta} \, \mathrm{d}\Gamma + \int_{\Gamma_u} \left[\boldsymbol{\sigma}^T\mathbf{P}_\nu - \mathbf{t}\right]^T \boldsymbol{\eta} \, \mathrm{d}\Gamma + \int_{\Gamma_u} [\bar{\mathbf{u}} - \mathbf{u}]^T \bar{\boldsymbol{\tau}} \, \mathrm{d}\Gamma = 0 \quad (4.12)$$

Since equation (4.12) has to be satisfied for any variations $\boldsymbol{\eta}$, $\boldsymbol{\gamma}$, $\boldsymbol{\tau}$ and $\bar{\boldsymbol{\eta}}$; the Euler–Lagrange equations, associated to the functional (4.7), are

$$\begin{aligned}
\mathbf{D}^T\boldsymbol{\sigma} + \mathbf{b}_v &= \mathbf{0} && \text{in } \Omega && \text{internal equilibrium} \\
\boldsymbol{\varepsilon} - \mathbf{Du} &= \mathbf{0} && \text{in } \Omega && \text{strain compatibility} \\
\boldsymbol{\sigma} - \tfrac{\partial\Psi}{\partial\boldsymbol{\varepsilon}} &= \mathbf{0} && \text{in } \Omega && \text{constitutive law} \\
\boldsymbol{\sigma}^T\mathbf{P}_\nu - \mathbf{t} &= \mathbf{0} && \text{on } \Gamma_u && \text{external equilibrium} \\
\bar{\mathbf{u}} - \mathbf{u} &= \mathbf{0} && \text{on } \Gamma_u && \text{essential boundary conditions} \\
\boldsymbol{\sigma}^T\mathbf{P}_\nu - \bar{\mathbf{t}} &= \mathbf{0} && \text{on } \Gamma_t && \text{natural boundary conditions}
\end{aligned} \quad (4.13)$$

Equations (4.13) are the governing equations of the boundary value problem for a continuous solid, figure 4.1. It may be shown that these equations satisfy the stationarity condition (4.6) of functional (4.7); but when a numerical method is used to obtain an approximate solution of them, they are satisfied only in an average sense, also referred as *weak form*, and not point to point, *strong form*.

It is important to point out that the functional (4.7) can give rise to a continuous field, in the entire domain of the solid, of each independent variable. This implies that the number of degrees of freedom (dof) of the problem is increased according to the total number of independent fields. In this case, for a three dimensional problem, each point considers three *dof* of displacements, six *dof* of strains, six *dof* of stresses and, if this point is on a boundary, three *dof* of tractions; in total 18 *dof*. In theory any solution by using the general *De Veubeke–Hu–Washizu* formulation can obtain continuous fields; but there exist an inconsistency when this occurs and was analyzed by *De Veubeke* as a limitation condition of mixed formulations [31].

Continuity requirements

Inspection of the functional (4.7) shows that it contains only first derivatives of the displacement field, because first order derivatives appear in the dependent field $\boldsymbol{\varepsilon} = \mathbf{Du}$. Whenever referring to the other three independent fields, the order of their derivatives is zero since the functional does not considers continuity of the their derivatives.

From this characterization, it follows that when the VHW principle in the form (4.7) is used to derive finite elements, the assumed displacements should be C^0 interelement continuous, whereas assumed strains and stresses can be discontinuous between elements.

4.1 A hierarchy of variational formulations

Starting from functional (4.7), it is possible to derive a hierarchy of variational formulations through considering fields which make that some equations defined in (4.13) are *a priori* satisfied, [87, 89, 91].

4.2 Three field formulation

If the tractions $\mathbf{t}$, are removed from the functional (4.7) by considering that essential boundary conditions are *a priori* satisfied, $\bar{\mathbf{u}} - \mathbf{u} = \mathbf{0}$, the following three field variational principle is obtained

$$\delta\Pi(\mathbf{u}, \boldsymbol{\varepsilon}, \boldsymbol{\sigma}) = \delta(U + P + D) = 0 \tag{4.14}$$

where Π is the three field functional given by

$$\Pi = \int_{\Omega} \left[\boldsymbol{\sigma}^T \left(\mathbf{D}\mathbf{u} - \boldsymbol{\varepsilon} \right) + \Psi(\boldsymbol{\varepsilon}) - \mathbf{u}^T \mathbf{b}_v \right] \, \mathrm{d}\Omega - \int_{\Gamma_t} \mathbf{u}^T \bar{\mathbf{t}} \, \mathrm{d}\Gamma \tag{4.15}$$

where only three independent fields are subject to variations: displacements $\mathbf{u}$, strains $\boldsymbol{\varepsilon}$ and stresses $\boldsymbol{\sigma}$. From this point, taking the variations of each independent field and applying the stationarity conditions (4.14), the corresponding Euler–Lagrange equations are defined by (4.13); but equations $(4.13)_4$ and $(4.13)_5$ do not appear any more. According to the aforementioned, in this formulation there are 15 *dof* per node for a three dimensional problem; named three displacements, six strains and six stresses.

4.3 Hellinger–Reissner Formulation

Other kind of variational formulation may be derived from the general VHW formulation by considering that the essential boundary conditions, equations $(4.13)_4$ and $(4.13)_5$, and the strain compatibility, equation $(4.13)_2$, are *a priori* satisfied. From these considerations the well known *Hellinger–Reissner* (HR) principle is recovered.

$$\delta\Pi(\mathbf{u}, \boldsymbol{\sigma}) = 0 \tag{4.16}$$

where Π is the Hellinger–Reissner functional

$$\Pi = \int_\Omega \left[\boldsymbol{\sigma}^T \left(\mathbf{Du} \right) - \hat{\Psi}(\boldsymbol{\sigma}) - \mathbf{u}^T \mathbf{b}_v \right] \mathrm{d}\Omega - \int_{\Gamma_t} \mathbf{u}^T \bar{\mathbf{t}} \, \mathrm{d}\Gamma \tag{4.17}$$

where $\hat{\Psi}(\sigma_x, \sigma_y, ..., \sigma_{xy})$, briefly denotes as $\hat{\Psi}(\boldsymbol{\sigma})$, is a state function, complementary energy density, defined by the Legendre transformation, [31, 76, 77, 113]

$$\int_\Omega \Psi(\boldsymbol{\varepsilon}) \, \mathrm{d}\Omega = \int_\Omega \boldsymbol{\sigma}^T \left(\mathbf{Du} \right) \mathrm{d}\Omega - \int_\Omega \hat{\Psi}(\boldsymbol{\sigma}) \, \mathrm{d}\Omega \tag{4.18}$$

which introduces the condition that $\boldsymbol{\varepsilon} = \mathbf{Du}$. For this formulation two independent fields are introduced; the displacement field and the stress field. This implies than in a finite element formulation, it is possible to have stresses as *dof* at the nodes of an element.

4.4   Strain–displacement Reissner Principle

To derive the energy functional corresponding to the *Strain–Displacement Reissner Principle* (SDR), equation (4.17) is modified by introducing $\Psi(\boldsymbol{\varepsilon})$ in place of $\hat{\Psi}(\boldsymbol{\sigma})$ to obtain

$$\delta\Pi(\mathbf{u}, \boldsymbol{\varepsilon}) = 0 \tag{4.19}$$

and the functional Π is redefined as

$$\Pi = \int_\Omega \left[\boldsymbol{\sigma}^T \left(\mathbf{Du} \right) - \Psi(\boldsymbol{\varepsilon}) - \mathbf{u}^T \mathbf{b}_v \right] \mathrm{d}\Omega - \int_{\Gamma_t} \mathbf{u}^T \bar{\mathbf{t}} \, \mathrm{d}\Gamma \tag{4.20}$$

4.5   Principle of minimum potential energy

From the stationarity conditions (4.13) which are satisfied by the functional (4.7), in this section a principle, which considers only the displacement field subject to variation, is derived. Equations $(4.13)_2$, $(4.13)_4$, $(4.13)_5$ and $(4.13)_6$ are *a priori* satisfied and equation $(4.13)_3$ is not considered explicitly in the derivation of the functions but it may be taken into account by

$$\boldsymbol{\sigma} = \frac{\partial \Psi}{\partial \boldsymbol{\varepsilon}} \tag{4.21}$$

Equation (4.21) assures the existence of the strain energy density function $\Psi(\boldsymbol{\varepsilon})$ from which stresses are derived. This point introduces a limitation to this principle since it is now restricted to elastic bodies because displacements are related to stresses by means of a constitutive law whereas the principle of virtual displacements is valid for any constitutive law.

$$\delta\Pi(\mathbf{u}) = 0 \tag{4.22}$$

The corresponding functional is given by

$$\Pi = \int_{\Omega} \left[\Psi(\boldsymbol{\varepsilon}) - \mathbf{u}^T\mathbf{b}_v\right] \mathrm{d}\Omega - \int_{\Gamma_t} \mathbf{u}^T\bar{\mathbf{t}} \, \mathrm{d}\Gamma \tag{4.23}$$

The principle defined in (4.24) states that: *Among all admissible displacements* $\mathbf{u}$ *which satisfy the prescribed essential boundary conditions* $\bar{\mathbf{u}}$, *defined on* Γ_u, *the actual displacements make the total potential energy minimum.*

4.6 Principle of minimum complementary energy

Now it will be shown that another variational principle can be derived from the *Principle of Complementary Virtual Work* when equilibrium conditions for the stresses $\boldsymbol{\sigma}$ and the prescribed tractions $\bar{\mathbf{t}}$ along the element boundary are satisfied, functional (4.17) is reduced to the principle of minimum complementary energy with stresses $\boldsymbol{\sigma}$ as the only field variable

$$\delta\Pi(\boldsymbol{\sigma}) = 0 \tag{4.24}$$

where the energy functional Π is

$$\Pi = \int_{\Omega} \hat{\Psi}(\boldsymbol{\sigma}) \, \mathrm{d}\Omega - \int_{\Gamma_u} \mathbf{t}^T\bar{\mathbf{u}} \, \mathrm{d}\Gamma \tag{4.25}$$

This principle states that: *Among all the sets of admissible stresses* $\boldsymbol{\sigma}$ *which satisfy the equations of equilibrium and the prescribed natural boundary conditions* $\bar{\mathbf{t}}$, *defined on* Γ_t, *the set of actual stress components makes the total complementary energy, defined by equation (4.25), an absolute minimum.*

Chapter 5

Embedded discontinuity formulation

In the context of the approximation of the embedded discontinuity formulation, different approaches have been developed regarding the interpolation of displacement and strain fields. Some approaches, like that developed by Belytschko *et al.*, [18] departing from the *Assumed Enhanced Strain* method (EAS) [99], have been proved to be statically optimal, *i.e.*, traction continuity across the discontinuity, but do not reproduce properly the kinematics of the discontinuity, rigid body motions of the two parts in which the element is split by the discontinuity; this kind of approaches has been classified as *Statically Optimal Symmetric* (SOS) in a comprehensive study made by Jirásek [55].

Another kind of approaches where the kinematics of strain is derived in a consistent form from the displacement field, corresponds to those developed by Lotfi and Shing [69] and Juárez and Ayala [59, 60]. In these formulations, the kinematics allows to capture the rigid body motions of the two parts in which the element is divided by the discontinuity; furthermore the traction continuity is not enforced at elemental level, in a strong form, since this condition emerges in a natural way from the variational formulation. Strictly speaking, when the width of the localization zone collapses into a line, the traction continuity is not imposed properly and is satisfied only in weak form. Jirásek [55] classifies these approaches as *Kinematically Optimal Symmetric* (KOS).

Alternately to the formulations previously described, there exists other kind of approaches where both the kinematics of the discontinuity and the traction continuity across the discontinuity are satisfied. These approaches are developed from the (EAS) method [102] considering a Petrov–Galerkin type formulation leading to a nonsymmetric formulation of the problem. Examples of these approaches are those developed by Simo *et al.* [101], Oliver [78, 79], Armero and Garikipati [8] and Wells and Sluys [116]. These approaches are named *Kinematically and Statically Nonsymmetric* (KSON) formulations by Jirásek [55].
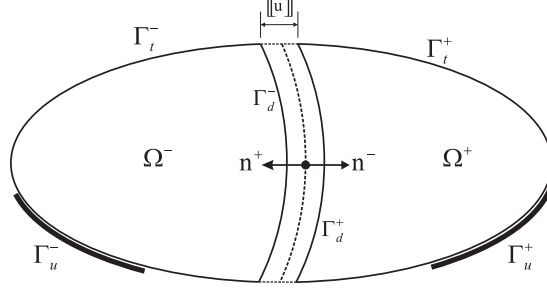
Figure 5.1: Continuum divided in Ω^- and Ω^+ by a discontinuity Γ_d.

5.1 Kinematically optimal symmetric formulation

As stated before, there are three different formulations of the embedded discontinuity model. In this work only the KOS formulation is addressed; regarding its discrete approach. For a comparative study of the results, derived from the numerical tests, additionally the KSON formulation has been implemented. Both formulations are developed for two dimensional analyses with the *constant strain triangle* (CST) element under quasi-static load conditions for the mode I of failure.

5.1.1 Three field formulation

Once the energy functional for a continuum solid is established, it is possible to take into account the dissipation energy on the discontinuity boundary Γ_d, [87, 89]. For this, consider a solid divided by Γ_d in Ω^- and Ω^+, figure 5.1, where the normal to the discontinuity is given by $\mathbf{n}$ and the relative displacement between both subdomains is defined by the jump $[\![\mathbf{u}]\!]$ in the displacements field $\mathbf{u}$. The energy functional for this solid is written from equation (4.15) as,

$$\Pi(\mathbf{u}, \boldsymbol{\varepsilon}, \boldsymbol{\sigma}, [\![\mathbf{u}]\!]) = \int_\Omega \left[\boldsymbol{\sigma}^T \left(\mathbf{D}\mathbf{u} - \boldsymbol{\varepsilon} \right) + \Psi(\boldsymbol{\varepsilon}) - \mathbf{u}^T \mathbf{b}_v \right] \, \mathrm{d}\Omega - \int_{\Gamma_t} \mathbf{u}^T \bar{\mathbf{t}} \, \mathrm{d}\Gamma +$$
$$\int_{\Gamma_d} \psi([\![\mathbf{u}]\!]) \, \mathrm{d}\Gamma \tag{5.1}$$

where $\psi([\![\mathbf{u}]\!])$ is an additional term which considers the elastic free energy density defined on the discontinuity Γ_d, derived from the field $[\![\mathbf{u}]\!]$. For a discontinuity with an elastic behavior, this function is given by

$$\psi([\![\mathbf{u}]\!]) = \int_0^{[\![\mathbf{u}]\!]} \mathbf{t}^T \, \mathrm{d}[\![\mathbf{u}]\!] \tag{5.2}$$

where $\mathbf{t}$ are the tractions on the discontinuity derived from a cohesive constitutive law traction–jump, $\mathbf{t} = \mathbf{T}[\![\mathbf{u}]\!]$; furthermore, for a discontinuity with a linear elastic behavior, this function is rewritten as

$$\psi([\![\mathbf{u}]\!]) = \frac{1}{2}[\![\mathbf{u}]\!]^T \mathbf{T}[\![\mathbf{u}]\!] \tag{5.3}$$

Hence the functional involves four independent fields. Now the first variation of the functional considering each of the four independent field is obtained as

$$\delta\Pi = \int_\Omega \left[(\mathbf{D}\mathbf{u} - \boldsymbol{\varepsilon})^T \boldsymbol{\tau} + \left(\frac{\partial\Psi}{\partial\boldsymbol{\varepsilon}} - \boldsymbol{\sigma} \right)^T \boldsymbol{\gamma} + \boldsymbol{\sigma}^T (\mathbf{D}\boldsymbol{\eta}) - \mathbf{b}_v^T \boldsymbol{\eta} \right] d\Omega -$$
$$\int_{\Gamma_t} \bar{\mathbf{t}}^T \boldsymbol{\eta}\, d\Gamma + \int_{\Gamma_d} \left(\frac{\partial\psi}{\partial[\![\mathbf{u}]\!]} \right)^T \tilde{\boldsymbol{\eta}}\, d\Gamma = 0 \tag{5.4}$$

for all variations $(\boldsymbol{\eta}, \boldsymbol{\gamma}, \boldsymbol{\tau})$, already defined in chapter 4, and $\tilde{\boldsymbol{\eta}}$ is the variation of the displacement jump $[\![\mathbf{u}]\!]$. Applying the divergence theorem, see appendix B, to the term $\int_\Omega \boldsymbol{\sigma}^T (\mathbf{D}\boldsymbol{\eta})\, d\Omega$ and dividing the domain Ω into Ω^- and Ω^+,

$$\int_\Omega \boldsymbol{\sigma}^T (\mathbf{D}\boldsymbol{\eta})\, d\Omega = -\int_{\Omega^-} (\boldsymbol{\sigma}^T\mathbf{D})\, \boldsymbol{\eta}^-\, d\Omega - \int_{\Omega^+} (\boldsymbol{\sigma}^T\mathbf{D})\, \boldsymbol{\eta}^+\, d\Omega + \int_{\Gamma_t^-} (\boldsymbol{\sigma}^T\mathbf{P}_\nu)\, \boldsymbol{\eta}^-\, d\Gamma$$
$$+ \int_{\Gamma_t^+} (\boldsymbol{\sigma}^T\mathbf{P}_\nu)\, \boldsymbol{\eta}^+\, d\Gamma + \int_{\Gamma_d^-} (\boldsymbol{\sigma}^T\mathbf{P}_n)\, \boldsymbol{\eta}^-\, d\Gamma - \int_{\Gamma_d^+} (\boldsymbol{\sigma}^T\mathbf{P}_n)\, \boldsymbol{\eta}^+\, d\Gamma \tag{5.5}$$

where $\mathbf{P}_n$ is the normal–projection matrix, defined in the same form as the matrix $\mathbf{P}_n$, which contains the components of the normal vector $\mathbf{n}$. The substitution of equation (5.5) into (5.4) leads to conclude that the functional stated by equation (5.1) satisfies in weak form:

$$
\begin{array}{llll}
\mathbf{D}^T\boldsymbol{\sigma} + \mathbf{b}_v = \mathbf{0} & \text{in } \Omega & \text{internal equilibrium} \\
\boldsymbol{\varepsilon} - \mathbf{D}\mathbf{u} = \mathbf{0} & \text{in } \Omega & \text{strain compatibility} \\
\boldsymbol{\sigma} - \frac{\partial\Psi}{\partial\boldsymbol{\varepsilon}} = \mathbf{0} & \text{in } \Omega & \text{constitutive law} \\
\boldsymbol{\sigma}^T\mathbf{P}_\nu - \bar{\mathbf{t}} = \mathbf{0} & \text{on } \Gamma_t & \text{natural boundary conditions}
\end{array} \tag{5.6}
$$

The above field equations and boundary conditions are supplemented by the following equilibrium conditions across the discontinuity:

$$
\begin{array}{ll}
\mathbf{t} = -\left(\boldsymbol{\sigma}^+\right)^T \mathbf{P}_n^+ & \text{on } \Gamma_d \\
\mathbf{t} = \left(\boldsymbol{\sigma}^-\right)^T \mathbf{P}_n^- & \text{on } \Gamma_d
\end{array} \tag{5.7}
$$

5.1.2 Strain–displacement formulation

If the *constitutive law*, equation (5.6) $_3$, is imposed in strong form the functional corresponding to the strain–displacement formulation is recovered,

$$\Pi(\mathbf{u}, \boldsymbol{\varepsilon}, [\![\mathbf{u}]\!]) = \int_{\Omega} \left[\boldsymbol{\sigma}^T (\mathbf{Du}) - \Psi(\boldsymbol{\varepsilon}) - \mathbf{u}^T \mathbf{b}_v \right] d\Omega - \int_{\Gamma_t} \mathbf{u}^T \bar{\mathbf{t}} \, d\Gamma + \int_{\Gamma_d} \psi([\![\mathbf{u}]\!]) \, d\Gamma \quad (5.8)$$

5.1.3 Displacement formulation

In the same way as for the strain–displacement formulation here in equation (4.13) it is assumed that *strain compatibility*, equation (5.6) $_2$, and *constitutive law*, equation (5.6) $_3$, are satisfied in strong form,

$$\Pi(\mathbf{u}, [\![\mathbf{u}]\!]) = \int_{\Omega} \left[\Psi(\boldsymbol{\varepsilon}) - \mathbf{u}^T \mathbf{b}_v \right] d\Omega - \int_{\Gamma_t} \mathbf{u}^T \bar{\mathbf{t}} \, d\Gamma + \int_{\Gamma_d} \psi([\![\mathbf{u}]\!]) \, d\Gamma \quad (5.9)$$

5.2 Finite element approximation

Once the functional of the embedded discontinuity formulation for its discrete approach is defined; the discretization of the domain by the finite element method is carried out, using the displacement and strain kinematics developed in chapter 2, this is,

$$\mathbf{u} = \mathbf{N}\hat{\mathbf{u}} + \mathbf{N}_c \tilde{\mathbf{u}} \quad (5.10)$$

$$\mathbf{Du} = \mathbf{B}\hat{\mathbf{u}} + \mathbf{B}_c \tilde{\mathbf{u}} \quad (5.11)$$

where $\hat{\mathbf{u}}$ and $\tilde{\mathbf{u}}$ are the respective regular and not regular displacements, related with the jump $[\![\mathbf{u}]\!]$. The matrix $\mathbf{N}$ contains the standard shape functions, and the shape functions associated to the nodes which belong to the subdomain Ω^+ are contained in the matrix $\mathbf{N}_c$, chapter 2. As for the standard finite element method, here the matrices $\mathbf{B}$ and $\mathbf{B}_c$ contain the derivatives of the corresponding shape functions $\mathbf{N}$ and $\mathbf{N}_c$

5.2.1 Three field approximation

For this approximation, in addition to the interpolated fields of equations (5.10) and (5.11), the strain and stress independent fields are interpolated as follow

$$\boldsymbol{\varepsilon} = \mathbf{N}_e \, \mathrm{e} \tag{5.12}$$

$$\boldsymbol{\sigma} = \mathbf{N}_s \, \mathrm{s} \tag{5.13}$$

where $\mathbf{N}_e$ and $\mathbf{N}_s$ are to the interpolation functions of strains and stresses respectively, $\mathbf{e}$ is the vector of nodal strains, and $\mathbf{s}$ is the vector of nodal stresses. Substitution of equations (5.10) to (5.13) into (5.1) and its posterior minimization leads to:

$$\begin{bmatrix} \mathbf{K}_{ee} & \mathbf{K}_{es} & \mathbf{0} & \mathbf{0} \\ \mathbf{K}_{es}^T & \mathbf{0} & \mathbf{K}_{s\hat{u}} & \mathbf{K}_{s\tilde{u}} \\ \mathbf{0} & \mathbf{K}_{s\hat{u}}^T & \mathbf{0} & \mathbf{0} \\ \mathbf{0} & \mathbf{K}_{s\tilde{u}}^T & \mathbf{0} & \mathbf{K}_{\tilde{u}\tilde{u}} \end{bmatrix} \begin{Bmatrix} \mathbf{e} \\ \mathbf{s} \\ \hat{\mathbf{u}} \\ \tilde{\mathbf{u}} \end{Bmatrix} = \begin{Bmatrix} \mathbf{0} \\ \mathbf{0} \\ \mathbf{f}^{ext} \\ \mathbf{0} \end{Bmatrix} \tag{5.14}$$

where

$$\mathbf{K}_{ee} = \int_{\Omega} \mathbf{N}_e^T \mathbf{C} \mathbf{N}_e \, \mathrm{d}\Omega \tag{5.15}$$

$$\mathbf{K}_{es} = -\int_{\Omega} \mathbf{N}_e^T \mathbf{N}_s \, \mathrm{d}\Omega \tag{5.16}$$

$$\mathbf{K}_{s\hat{u}} = \int_{\Omega} \mathbf{N}_s^T \mathbf{B} \, \mathrm{d}\Omega \tag{5.17}$$

$$\mathbf{K}_{s\tilde{u}} = \int_{\Omega} \mathbf{N}_s^T \mathbf{B}_c \, \mathrm{d}\Omega \tag{5.18}$$

$$\mathbf{K}_{\tilde{u}\tilde{u}} = \int_{\Gamma_d} \mathbf{N}_c^T \mathbf{T} \mathbf{N}_c \, \mathrm{d}\Gamma \tag{5.19}$$

$$\mathbf{f}^{ext} = \int_{\Omega} \mathbf{N}^T \mathbf{b}_v \, \mathrm{d}\Omega + \int_{\Gamma_t} \mathbf{N}^T \bar{\mathbf{t}} \, \mathrm{d}\Gamma \tag{5.20}$$

33

From the algebraic equations system (5.14) it may be shown than the KOS formulation leads to a symmetric matrix and that the nonlinear behavior only appears in the submatrix $\mathbf{K}_{\tilde{u}\tilde{u}}$ since the rest of the submatrices are considered to remain elastic. Other important issue to point out, for this kind of mixed formulations, is that the matrix has zeros along its leading diagonal. The handling of this particular configuration requires the use of special solvers like those by *Linear Algebra Package* (LAPACK) [5, 35, 47].

To obtain stable mixed formulation, there are two important points to take into consideration, solvability and stability, both directly related with the Babuška–Brezzi condition [12, 23, 117, 118]. In appendix C these conditions are addressed to guarantee the convergence and the stability of these formulations.

5.2.2   Strain–displacement approximation

For this approach, the displacement and the independent strain fields are interpolated by means of equations (5.10) and (5.12), respectively; and the strain field, $\boldsymbol{\varepsilon}(\mathbf{u}) = \boldsymbol{\varepsilon}^u$, dependent of the displacement field $\mathbf{u}$, is derived according to equation (5.11). Substituting these three equations into the functional (5.8) and following the same step as for the last formulation,

$$
\begin{bmatrix}
-\mathbf{K}_{ee} & \mathbf{K}_{e\hat{u}} & \mathbf{K}_{e\tilde{u}} \\
\mathbf{K}_{e\hat{u}}^T & \mathbf{0} & \mathbf{0} \\
\mathbf{K}_{e\tilde{u}}^T & \mathbf{0} & \mathbf{K}_{\tilde{u}\tilde{u}}
\end{bmatrix}
\left\{
\begin{array}{c}
\mathbf{e} \\
\hat{\mathbf{u}} \\
\tilde{\mathbf{u}}
\end{array}
\right\}
=
\left\{
\begin{array}{c}
\mathbf{0} \\
\mathbf{f}^{ext} \\
\mathbf{0}
\end{array}
\right\}
\tag{5.21}
$$

where

$$
\mathbf{K}_{e\hat{u}} = \int_{\Omega} \mathbf{N}_e^T \mathbf{C} \mathbf{B} \, d\Omega
\tag{5.22}
$$

$$
\mathbf{K}_{e\tilde{u}} = \int_{\Omega} \mathbf{N}_e^T \mathbf{C} \mathbf{B}_c \, d\Omega
\tag{5.23}
$$

The other submatrices have been already defined. Considerations done to the *Three fields* formulation apply here since the particular configuration of the coefficient matrix, equation (5.21), is the same.

5.2.3   Displacement approximation

The substitution of equations (5.10) and (5.11) into the functional given by equation (5.9) and its corresponding minimization, leads to the next algebraic system of equations

$$
\begin{bmatrix} \mathbf{K}_{\hat{u}\hat{u}} & \mathbf{K}_{\hat{u}\tilde{u}} \\ \mathbf{K}_{\hat{u}\tilde{u}}^T & \mathbf{K}_{\tilde{u}\tilde{u}} \end{bmatrix} \left\{ \begin{array}{c} \hat{\mathbf{u}} \\ \tilde{\mathbf{u}} \end{array} \right\} = \left\{ \begin{array}{c} \mathbf{f}^{ext} \\ \mathbf{0} \end{array} \right\}
\tag{5.24}
$$

where

$$
\mathbf{K}_{\hat{u}\hat{u}} = \int_\Omega \mathbf{B}^T \mathbf{C} \mathbf{B} \, \mathrm{d}\Omega
\tag{5.25}
$$

$$
\mathbf{K}_{\hat{u}\tilde{u}} = \int_\Omega \mathbf{B}^T \mathbf{C} \mathbf{B}_c \, \mathrm{d}\Omega
\tag{5.26}
$$

$$
\mathbf{K}_{\tilde{u}\tilde{u}} = \int_\Omega \mathbf{B}_c^T \mathbf{C} \mathbf{B}_c \, \mathrm{d}\Omega + \int_{\Gamma_d} \mathbf{N}_c^T \mathbf{T} \mathbf{N}_c \, \mathrm{d}\Gamma
\tag{5.27}
$$

and the vector of external forces is given by equation (5.20). Here as for the mixed formulation, the coefficient matrix is symmetric and unlike the others there are no zeros along its leading diagonal and hence no special considerations have to be taken for choosing the solver used. The inelastic response is related to the term $\int_{\Gamma_d} \mathbf{N}_c^T \mathbf{T} \mathbf{N}_c \, \mathrm{d}\Gamma$ of the submatrix $\mathbf{K}_{\tilde{u}\tilde{u}}$.

5.3 Statically and kinematically optimal nonsymmetric formulation

In what follows an additional embedded discontinuity formulation like that presented in [1, 4] is introduced. For this, consider the principle of virtual work, for an elastic body, which states

$$
\int_\Omega \boldsymbol{\sigma}^T (\mathbf{D}\boldsymbol{\eta}) \, \mathrm{d}\Omega = \int_\Omega \left(\frac{\partial \Psi}{\partial \boldsymbol{\varepsilon}} \right)^T \mathbf{D}\boldsymbol{\eta} \, \mathrm{d}\Omega = \int_\Omega \mathbf{b}_v^T \boldsymbol{\eta} \, \mathrm{d}\Omega + \int_{\Gamma_t} \bar{\mathbf{t}}^T \boldsymbol{\eta} \, \mathrm{d}\Gamma
\tag{5.28}
$$

where $\boldsymbol{\sigma} = \frac{\partial \Psi}{\partial \boldsymbol{\varepsilon}}$ denotes the stresses derived from the constitutive law.

It can be shown that, integrating equation (5.28) by parts, equations (4.13)$_1$ and (4.13)$_4$ are obtained [79]. Thus, apart from the enforcement of the essential boundary conditions, the traction continuity of equation (5.7) still has to be imposed locally.

35

In previous works [8, 64, 101, 116] a mixed variational formulation is adopted in the framework of the *Assumed Enhanced Strain* (AES) method [102], from which the equilibrium as well as the traction continuity conditions are also derived. Wells [114] develops a formulation in the framework of the (AES) method in a detailed form.

Due to the bounded nature of the stress field, the stress vector is obtained from the continuum constitutive relation due to the regular part of the strain given by equation (2.15); hence:

$$\boldsymbol{\sigma} = \mathbf{C}\left(\mathbf{B}\hat{\mathbf{u}} + \mathbf{B}_c\tilde{\mathbf{u}}\right) \tag{5.29}$$

where $\mathbf{C}$ is the continuum constitutive tensor.

The discretized set of equations corresponding to the finite element approximation of (5.28) is,

$$\int_{\Omega} \mathbf{B}^T \boldsymbol{\sigma}\, \mathrm{d}\Omega = \mathbf{f}^{ext} \tag{5.30}$$

As mentioned before, to complete the set of equations (5.30) the traction continuity condition (5.7) still has to be enforced locally. In a weak form, the traction continuity condition can be written as:

$$\int_{\Omega} \mathbf{G}^T \boldsymbol{\sigma}\, \mathrm{d}\Omega + \int_{\Gamma_d} \mathbf{t}\, \mathrm{d}\Gamma = \mathbf{0} \tag{5.31}$$

where $\mathbf{t}$ is the traction vector obtained at the discontinuity Γ_d, matrix $\mathbf{G}$ is given by

$$\mathbf{G} = -\frac{l_d}{\Omega}\mathbf{P}_n = -\frac{l_d}{\Omega}\begin{bmatrix} n_1 & 0 \\ 0 & n_2 \\ n_2 & n_1 \end{bmatrix} \tag{5.32}$$

and l_d is the length of the discontinuity Γ_d. The traction vector $\mathbf{t}$ has to be derived from a discrete constitutive relation for the crack Γ_d according to the material model introduced in chapter 3 as:

$$\mathbf{t} = \mathbf{T}[\![\mathbf{u}]\!] \tag{5.33}$$

From the substitution of equation (5.32) into (5.31) it is possible to write

36

$$\frac{1}{l_d} \int_{\Gamma_d} \mathbf{t} \, \mathrm{d}\Gamma - \frac{1}{\Omega} \int_{\Omega} \boldsymbol{\sigma}^T \mathbf{P}_n \, \mathrm{d}\Omega = \mathbf{0} \tag{5.34}$$

which shows that the traction boundary condition is enforced in average. In the approximation considered, where constant strain triangles are adopted, equations (5.31) and (5.34) enforce traction continuity locally since, within each element, the functions in the integrals are constant. Moreover, in this particular case it can also be seen from equation (5.34) that the formulation does not depend upon the length l_d of the discontinuity Γ_d, [1, 4, 8, 79, 116].

Substituting the interpolated fields given by equation (5.29) into (5.30) and imposing at elemental level traction continuity given by (5.31) gives,

$$\begin{bmatrix} \mathbf{K}_{\hat{u}\hat{u}} & \mathbf{K}_{\hat{u}\tilde{u}} \\ \mathbf{K}_{\tilde{u}\hat{u}} & \mathbf{K}_{\tilde{u}\tilde{u}} \end{bmatrix} \begin{Bmatrix} \hat{\mathbf{u}} \\ \tilde{\mathbf{u}} \end{Bmatrix} = \begin{Bmatrix} \mathbf{f}^{ext} \\ \mathbf{0} \end{Bmatrix} \tag{5.35}$$

where

$$\mathbf{K}_{\tilde{u}\hat{u}} = \int_{\Omega} \mathbf{G}^T \mathbf{C} \mathbf{B} \, \mathrm{d}\Omega \tag{5.36}$$

$$\mathbf{K}_{\tilde{u}\tilde{u}} = \int_{\Omega} \mathbf{G}^T \mathbf{C} \mathbf{B}_c \, \mathrm{d}\Omega + \int_{\Gamma_d} \mathbf{T} \, \mathrm{d}\Gamma \tag{5.37}$$

and the other submatrices have been already defined.

Chapter 6

Equilibrium on the discontinuity boundary

The interpolation of the displacement jump field by the finite element method of the (KOS) formulation, developed in section 5.2, takes into account the shape function $\mathbf{N}_c$ given by equation (2.12). This kind of interpolation is a proper way to consider that the localization band width b_d is different from zero; but when this band collapses into a line, *i.e.,* a discrete discontinuity, the $\mathbf{N}_c$ functions have the meaning of the identity matrix which leads to consider only tractions at the discontinuity in the local framework.

The particular case, $b_d = 0$, may lead to a non proper imposition of the traction continuity which only satisfies equilibrium for some particular cases. To check this, the element shown in figure 6.1 is considered; here the discontinuity Γ_d crosses the element parallel to the side $1 - 2$, additionally l_{12} is the length of this side, $\mathbf{n}$ is the normal to the discontinuity and h is the height of the triangle. The angle β is measured from the x axis and the side $1 - 2$, and finally α is the angle between the x axis and the normal to the referred side.

The area of the element is $A = \frac{l_{12}\,h}{2}$, hence $2A = l_{12}\,h$, and from the geometry of the element and the angle β the following relations are obtained,

$$\cos\beta = \frac{x_2 - x_1}{l_{12}} \tag{6.1}$$

$$\sin\beta = \frac{y_2 - y_1}{l_{12}} \tag{6.2}$$

Furthermore, for the element shown in figure 6.1, the matrix $\mathbf{B}_c$ is defined as:

$$\mathbf{B}_c = -\frac{1}{2A} \begin{bmatrix} y_1 - y_2 & 0 \\ 0 & x_2 - x_1 \\ x_2 - x_1 & y_1 - y_2 \end{bmatrix} \tag{6.3}$$
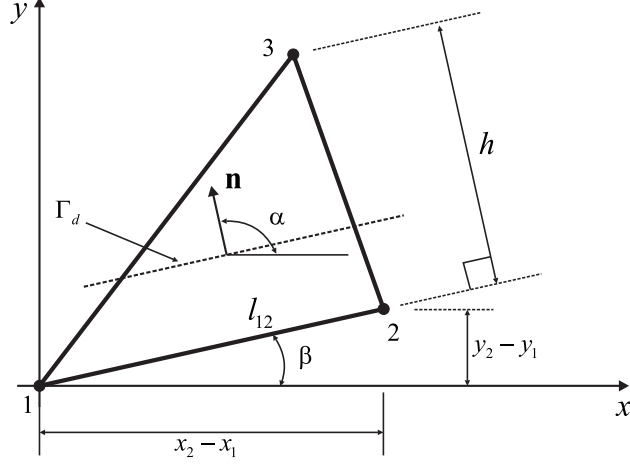
Figure 6.1: Discontinuity projected parallel to the opposite side to the solitary node.

rewriting the matrix $\mathbf{B}_c$ according to relations obtained from the geometry of the element and using the angle α instead of β,

$$\mathbf{B}_c = -\frac{1}{h} \begin{bmatrix} \cos\alpha & 0 \\ 0 & \sin\alpha \\ \sin\alpha & \cos\alpha \end{bmatrix} \tag{6.4}$$

The form of the matrix $\mathbf{B}_c$, equation (6.4), is similar to that for the normal–projection matrix, defined in appendix B, which contains the components of the vector $\mathbf{n}$, normal to the surface Γ_d,

$$\mathbf{P}_n = \begin{bmatrix} \cos\alpha & 0 \\ 0 & \sin\alpha \\ \sin\alpha & \cos\alpha \end{bmatrix} \tag{6.5}$$

The principal difference between equations (6.4) and (6.5) is the term $\frac{1}{h}$ which makes that the traction continuity can not be imposed correctly. Once a discontinuity appears the following equality has to be satisfied,

$$\int_\Omega \mathbf{B}_c^T \left(\boldsymbol{\sigma}^{\tilde{u}} + \underbrace{\boldsymbol{\sigma}^{\hat{u}}}_{\approx 0} \right) d\Omega + \int_{\Gamma_d} \mathbf{t}\, d\Gamma = \mathbf{0} \tag{6.6}$$

hence the equilibrium at the discontinuity depends only on the stresses coming from the regular displacement field $\boldsymbol{\sigma}^{\tilde{u}}$ and the tractions from the discontinuity. After some algebraic operations it may be shown than the tractions are expressed as

40

$$t_n = \frac{1}{2\,l_d}\left[y_1 - y_2\right]\sigma_{xx} \tag{6.7}$$

$$t_s = \frac{1}{2\,l_d}\left[x_2 - x_1\right]\sigma_{yy} \tag{6.8}$$

These results show that traction continuity is not satisfied since, the correct tractions are $t_n = \sigma_{xx}$ and $t_s = \sigma_{yy}$. Traction continuity is only recovered for special cases when $2\,l_d = (y_1 - y_2)$ and $2\,l_d = (x_2 - x_1)$. These conditions may lead to a stress locking problem in the element.

6.1 A correct definition of the discontinuity length

In what follows, a consistent way for a correct enforcement of equilibrium on the discontinuity surface is shown by means of some geometrical relationships. The formulation is developed for a constant strain triangle with the discrete approach of the symmetric embedded discontinuity model.

The system to solve is:

$$\begin{bmatrix} \mathbf{K}_{\hat{u}\hat{u}} & \mathbf{K}_{\hat{u}\tilde{u}} \\ \mathbf{K}_{\hat{u}\tilde{u}}^{T} & \mathbf{K}_{\tilde{u}\tilde{u}} \end{bmatrix} \left\{ \begin{matrix} \hat{\mathbf{u}} \\ \tilde{\mathbf{u}} \end{matrix} \right\} = \left\{ \begin{matrix} \mathbf{f}^{ext} \\ \mathbf{0} \end{matrix} \right\} \tag{6.9}$$

where

$$\mathbf{K}_{\hat{u}\hat{u}} = \int_{\Omega} \mathbf{B}^{T}\mathbf{C}\mathbf{B}\,\mathrm{d}\Omega \tag{6.10}$$

$$\mathbf{K}_{\hat{u}\tilde{u}} = \int_{\Omega} \mathbf{B}^{T}\mathbf{C}\mathbf{B}_{c}\mathbf{R}\,\mathrm{d}\Omega \tag{6.11}$$

$$\mathbf{K}_{\tilde{u}\tilde{u}} = \int_{\Omega} \mathbf{R}^{T}\mathbf{B}_{c}^{T}\mathbf{C}\mathbf{B}_{c}\mathbf{R}\,\mathrm{d}\Omega + \int_{\Gamma_d} \mathbf{N}_{c}^{T}\mathbf{T}\mathbf{N}_{c}\,\mathrm{d}\Gamma \tag{6.12}$$

and $\mathbf{R}$ is the rotation matrix from local coordinates to global coordinates defined as
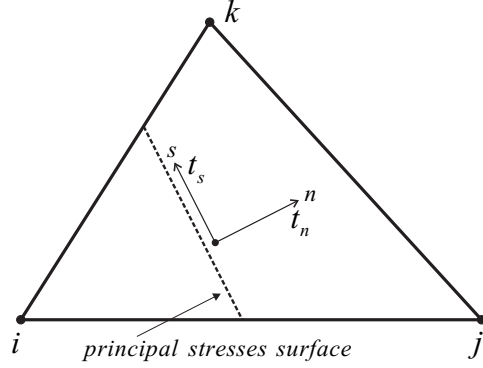
Figure 6.2: Principal stresses surface.

$$\mathbf{R} = \begin{bmatrix} \cos\theta & -\sin\theta \\ \sin\theta & \cos\theta \end{bmatrix} \tag{6.13}$$

The solution of the system of equations (6.9) leads to the equilibrium of the element in two parts. The first equation, (6.9)a, gives the equilibrium in nodes of the element and the second, (6.9)b, states the equilibrium of tractions on the internal discontinuity boundary as:

$$\int_{\Omega} \mathbf{R}^T \mathbf{B}_c^T (\boldsymbol{\sigma}^{\tilde{u}} + \boldsymbol{\sigma}^{\hat{u}}) \, \mathrm{d}\Omega + \int_{\Gamma_d} \mathbf{t} \, \mathrm{d}\Gamma = \mathbf{0} \tag{6.14}$$

From equation (6.14) it is possible to see that the equilibrium is imposed between the tractions $\mathbf{t}$ defined on the discontinuity Γ_d and the internal forces of the solitary node i, figure 6.4.

Figure 6.3: Geometrical relationships for the construction of the matrix $\mathbf{B}_c$.
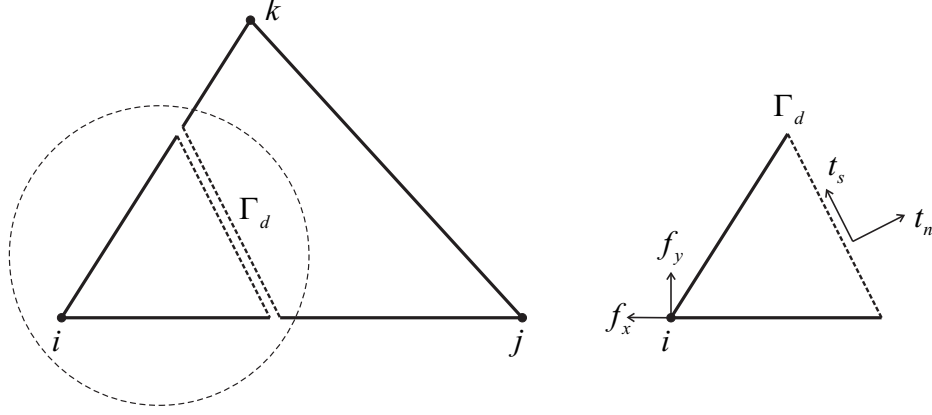
Figure 6.4: Tractions equilibrium on the discontinuity boundary Γ_d.

According to the construction of the matrix $\mathbf{B}_c$, which is derived from the geometry of the element, the correct imposition of the equilibrium on the discontinuity occurs only in a particular surface which defines the geometry of the discontinuity.

This point makes the formulation directly dependent on the location of the discontinuity in the element; unlike the nonsymmetric formulation [1, 54, 78, 114], where the sol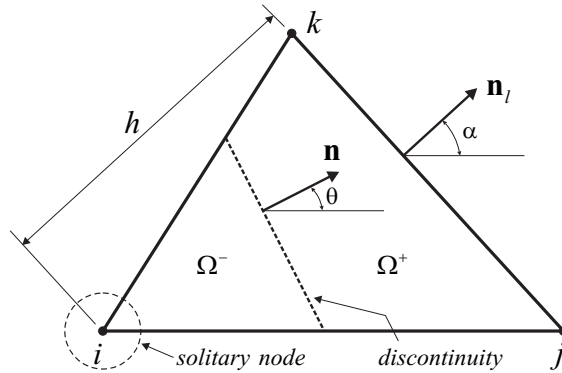ution is invariant with respect to the geometry of the discontinuity. From this condition, the localization of the discontinuity is a variable in the problem for the symmetric embedded discontinuity formulation, figure 6.3.

The aim of this analysis is to find the surface Γ_d where evaluation of equation (6.14) guarantees the equilibrium of tractions across the discontinuity. The initial conditions, in the moment in which, $\boldsymbol{\sigma}_I > \sigma_{t0}$, are:

$$
\begin{aligned}
t_n &= \sigma_{t0} = \sigma_I \\
t_s &= 0 \\
[\![\mathbf{u}]\!] &\approx 0
\end{aligned}
\tag{6.15}
$$

with σ_I being the principal stress I and σ_{t0} the strength of the material. These initial conditions lead to the following form of equation (6.14):

$$
t_n \, l_d = \frac{A}{h}\left[\cos\theta(\cos\alpha\,\sigma_x + \sin\alpha\,\sigma_{xy}) + \sin\theta(\sin\alpha\,\sigma_y + \cos\alpha\,\sigma_{xy})\right]
\tag{6.16}
$$

Equation (6.16) contains *sine* and *cosine* functions which can be transformed by means of some trigonometric identities; additionally the shear stress is

$$
\sigma_{xy} = \frac{1}{2}\tan 2\theta(\sigma_x - \sigma_y)
\tag{6.17}
$$

43

Substitution of equation (6.17) into equation (6.16) leads to

$$t_n \frac{l_d\,h}{A} = \frac{1}{2}\left[\cos\left(\theta+\alpha\right)(\sigma_x-\sigma_y)+\cos\left(\theta-\alpha\right)(\sigma_x+\sigma_y)+\tan 2\theta \sin\left(\theta+\alpha\right)(\sigma_x-\sigma_y)\right] \quad (6.18)$$

grouping similar terms in this last equation,

$$t_n \frac{l_d\,h}{A} = \frac{1}{2}\left[(\sigma_x-\sigma_y)\Big(\cos\left(\theta+\alpha\right)+\tan 2\theta \sin\left(\theta+\alpha\right)\Big)+(\sigma_x+\sigma_y)\cos\left(\theta-\alpha\right)\right] \quad (6.19)$$

now dividing both sides of equation (6.19) by $\cos\left(\theta-\alpha\right)$,

$$t_n \frac{l_d\,h}{A}\frac{1}{\cos\left(\theta-\alpha\right)} = \frac{1}{2}\left[\frac{(\sigma_x-\sigma_y)}{\cos\left(\theta-\alpha\right)}\left(\cos\left(\theta+\alpha\right)+\tan 2\theta \sin\left(\theta+\alpha\right)\right)+(\sigma_x+\sigma_y)\right] \quad (6.20)$$

And the initial condition $t_n = \sigma_I$ implies that the right hand side of equation (6.20) has to be equal to σ_I. This is true if and only if the first term is equal to:

$$\cos\left(\theta+\alpha\right)+\tan 2\theta \sin\left(\theta+\alpha\right) = \sqrt{1+\tan^2 2\theta}\,\cos\left(\theta-\alpha\right) \quad (6.21)$$

To prove this equality, both sides of equation (6.21) are squared to obtain

$$\cos^2\left(\theta+\alpha\right)+2\cos\left(\theta+\alpha\right)\tan 2\theta \sin\left(\theta+\alpha\right)+\tan^2 2\theta \sin^2\left(\theta+\alpha\right) = \\ (1+\tan^2 2\theta)\cos^2\left(\theta-\alpha\right) \quad (6.22)$$

After some algebraic work considering trigonometric identities, the following equation is derived

$$\sin 2\theta \sin 2\alpha = \sin 2\theta \sin 2\alpha \quad (6.23)$$

proving the equality (6.21). Once the equality (6.21) has been proved, the next step is to replace the right hand side of equation (6.20) by the principal stress σ_I and $t_n = \sigma_I$; according to this,

$$l_d = \frac{A}{h}\cos\left(\theta-\alpha\right) \quad (6.24)$$

Equation (6.24) defines the surface, inside the element, where imposition of tractions continuity, equation (6.14), guarantees the equilibrium along the discontinuity boundary Γ_d.

6.2 Alternative enforcement of equilibrium

From the observations made, to the transformation matrix $\mathbf{B}_c$, at the beginning of this chapter, there exists another form to the correct imposition of the equilibrium across the discontinuity boundary. According to the construction of this matrix, stresses are transmitted to a surface parallel to the side opposite to the solitary node i, figure 6.3; hence is it possible to obtain equilibrium at this surface if the length of the discontinuity is equal to

$$l_d = \frac{A}{h} \tag{6.25}$$

Imposition of traction continuity on the surface defined by equation (6.25), makes the formulation strongly dependent of the mesh configuration since the discontinuity has to be introduced parallel to one side of the element.

Chapter 7

Numerical implementation

The embedded discontinuity formulation consists essentially of adding, to the standard continuum finite elements, enhanced deformation modes controlled by additional degrees of freedom. Depending on the support of those additional deformation modes, the formulation may be split up into two types of implementation.

The first one considers an elemental enrichment (see for instance [4, 8, 9, 37, 68, 75, 80, 90]), *i.e.,* only elemental degrees of freedom are used to introduced the jump in the displacement field; in consequence, by taking advantage of the configuration of the system of algebraic equations, it is possible to perform an static condensation to eliminate the additional degrees of freedom, related with the displacement jump, preserving only the standard as for the classical FEM which is treated in the same way as inelastic strains are [74]. The resulting displacement jump field is piecewise continuous since there is not continuity across the elements boundaries.

In the second type of implementation, the support of the additional enhanced deformation modes are the standard FE nodes, *i.e.,* the number of degrees of freedom per node is increased by some additional, related with the displacement jump (two per node in 2D problems and three for 3D problems), see for instance [34, 73, 81, 103, 104, 115]. The final displacement jump field is continuous since the additional degrees of freedom are shared between elements and the static condensation is not possible because the resulting formulation is irreducible. This type of formulations, where the discontinuity is distributed in all the domain of the element, is commonly known as *Extended Finite Element Method* (XFEM) and is similar to the *Smeared Crack* formulation.

Unlike the first type of embedded discontinuity implementation, mentioned above, here the computational implementation is highly complicated since, the number of degrees of freedom of the elements which undergo localization has to be modified as soon as one of the candidate elements, ahead the discontinuity, violates the yield condition. This drawback makes these formulations not attractive for implementation because different types of elements have to be introduced in the mesh, standard elements or modified elements which consider the influence of the additional deformation modes. The computational cost associated with the enhancement of the element approximation, may be higher than

that involved in the solution of the problem of damage; similar to when interface elements are used to model a discrete crack propagation.

An alternative to the introduction of additional deformation modes in a global framework, is to introduce global nodes along the crack path to simulate continuous displacement jumps; therefore, these additional degrees of freedom are common between adjacent elements [3, 27, 28]. Both the crack path and the displacement jumps are continuous across element boundaries.

In this chapter, different points related with the numerical implementation of embedded discontinuity formulation, are addressed with special emphasis on those used for the adopted formulation. One of the main points in the numerical implementation, for reducible formulations, is the static condensation

In order to get insight the static condensation procedure, applied in the formulation developed in this work, in the following section two different forms to perform the static condensation are presented.

7.1   Static condensation

The first form to do the static condensation is in the classical way, which can be applied in the total form or incremental form of the resulting system of algebraic equations, where a common Gauss's elimination procedure is performed [72]. To do this, consider the incremental form of the system of algebraic equations, derived in chapter 5, for the displacement formulation

$$
\begin{bmatrix} \mathbf{K}_{\hat{u}\hat{u}} & \mathbf{K}_{\hat{u}\tilde{u}} \\ \mathbf{K}_{\hat{u}\tilde{u}}^T & \mathbf{K}_{\tilde{u}\tilde{u}} \end{bmatrix} \begin{Bmatrix} d\hat{\mathbf{u}} \\ d\tilde{\mathbf{u}} \end{Bmatrix} = \begin{Bmatrix} \mathbf{f}^{ext} \\ \mathbf{0} \end{Bmatrix} - \begin{Bmatrix} \mathbf{f}_{\hat{u}}^{int} \\ \mathbf{f}_{\tilde{u}}^{int} \end{Bmatrix}
\tag{7.1}
$$

with the internal forces defined as

$$
\mathbf{f}_{\hat{u}}^{int} = \int_{\Omega} \mathbf{B}^T \left(\boldsymbol{\sigma}^{\hat{u}} + \boldsymbol{\sigma}^{\tilde{u}} \right) \mathrm{d}\Omega
\tag{7.2}
$$

$$
\mathbf{f}_{\tilde{u}}^{int} = \int_{\Omega} \mathbf{B}_c^T \left(\boldsymbol{\sigma}^{\hat{u}} + \boldsymbol{\sigma}^{\tilde{u}} \right) \mathrm{d}\Omega + \int_{\Gamma_d} \mathbf{t} \, \mathrm{d}\Gamma
\tag{7.3}
$$

where $\boldsymbol{\sigma}^{\hat{u}}$ and $\boldsymbol{\sigma}^{\tilde{u}}$ are the stresses derived from the displacement $\hat{\mathbf{u}}$ and displacement jump $\tilde{\mathbf{u}}$ fields, respectively. The incremental forms of these fields are denoted by $d\hat{\mathbf{u}}$ and $d\tilde{\mathbf{u}}$. The other matrices were defined in chapter 5.

As can be observed from the system of equations (7.1), the problem is nonlinear in the variables $\hat{\mathbf{u}}$ and $\tilde{\mathbf{u}}$, which implies that an iterative solution strategy has to employed. A popular scheme is Newton's method [32, 53, 58, 62, 105, 109], where the solution is computed as a sequence of linear approximations, which may be summarized as:

1. Given the set of equations

   $$\mathbf{f}(\mathbf{x}) = \mathbf{0}$$

   where $\mathbf{x}$ are the dependent variables.

2. Construct the linear part of $\mathbf{f}$ about a current point $\mathbf{x}^{(i)}$ as

   $$\mathbf{f}^{(i+1)} \approx \mathbf{f}^{(i)} + \frac{\partial \mathbf{f}}{\partial \mathbf{x}}\Big|_{\mathbf{x}=\mathbf{x}^{(i)}} d\mathbf{x}^{(i+1)} = \mathbf{0}$$

   where $d\mathbf{x}^{(i+1)}$ is an increment of $\mathbf{x}$.

3. Solve the linear problem

   $$d\mathbf{x}^{(i+1)} = -\left(\mathbf{F}^{(i)}\right)^{-1}\mathbf{f}^{(i)}; \quad \mathbf{F}^{(i)} = \frac{\partial \mathbf{f}}{\partial \mathbf{x}}\Big|_{\mathbf{x}=\mathbf{x}^{(i)}}$$

   and update the solution as

   $$\mathbf{x}^{(i+1)} = \mathbf{x}^{(i)} + d\mathbf{x}^{(i+1)}$$

   In the above $\mathbf{F}^{(i)}$ is the *Jacobian* or tangent matrix for the equations.

4. Repeat steps 2 and 3 until the solution converges within a given tolerance.

Now the Newton's method is applied to the set of equations (7.1) as follows

$$
\begin{bmatrix} \mathbf{R}_{\hat{u}}^{(i+1)} \\ \mathbf{R}_{\tilde{u}}^{(i+1)} \end{bmatrix} \approx \begin{bmatrix} \mathbf{R}_{\hat{u}}^{(i)} \\ \mathbf{R}_{\tilde{u}}^{(i)} \end{bmatrix} - \begin{bmatrix} \mathbf{K}_{\hat{u}\hat{u}}^{(i)} & \mathbf{K}_{\hat{u}\tilde{u}}^{(i)} \\ \mathbf{K}_{\hat{u}\tilde{u}}^{T(i)} & \mathbf{K}_{\tilde{u}\tilde{u}}^{(i)} \end{bmatrix} \begin{bmatrix} d\hat{\mathbf{u}}^{(i+1)} \\ d\tilde{\mathbf{u}}^{(i+1)} \end{bmatrix}
$$
$$
= \begin{bmatrix} \hat{\mathbf{R}}_{\hat{u}}^{(i+1)} \\ \mathbf{0} \end{bmatrix}
$$

(7.4)

where

$$\mathbf{R}_{\hat{u}}^{(i)} = \mathbf{f}^{ext,(i+1)} - \mathbf{f}_{\hat{u}}^{int,(i)} \tag{7.5}$$

$$\mathbf{R}_{\tilde{u}}^{(i)} = -\mathbf{f}_{\tilde{u}}^{int,(i)} \tag{7.6}$$

In chapter 5 it was pointed out that the nonlinear behavior of the system is due to the submatrix $\mathbf{K}_{\tilde{u}\tilde{u}}$. This implies that

$$\mathbf{K}_{\hat{u}\hat{u}}^{(i)} = \mathbf{K}_{\hat{u}\hat{u}}; \quad \mathbf{K}_{\hat{u}\tilde{u}}^{(i)} = \mathbf{K}_{\hat{u}\tilde{u}} \quad \forall\, i = 1, 2, 3, \ldots \tag{7.7}$$

and the tangent stiffness matrix is defined as

$$\mathbf{K}_{\tilde{u}\tilde{u}}^{(i)} = -\left.\frac{\partial \mathbf{R}_{\tilde{u}}}{\partial \tilde{\mathbf{u}}}\right|^{(i)} \tag{7.8}$$

which expands to

$$\mathbf{K}_{\tilde{u}\tilde{u}}^{(i)} = \int_{\Omega} \mathbf{B}_c^T \left.\frac{\partial \boldsymbol{\sigma}^{\tilde{u}}}{\partial \boldsymbol{\varepsilon}}\right|^{(i)} \frac{\partial \boldsymbol{\varepsilon}}{\partial \tilde{\mathbf{u}}}\, \mathrm{d}\Omega + \int_{\Gamma_d} \left.\frac{\partial \mathbf{t}}{\partial \tilde{\mathbf{u}}}\right|^{(i)} \mathrm{d}\Gamma$$

$$= \int_{\Omega} \mathbf{B}_c^T \mathbf{C}_t^{(i)} \mathbf{B}_c\, \mathrm{d}\Omega + \int_{\Gamma} \mathbf{T}_t^{(i)}\, \mathrm{d}\Gamma \tag{7.9}$$

where

$$\mathbf{T}_t^{(i)} = \left.\frac{\partial \mathbf{t}}{\partial \tilde{\mathbf{u}}}\right|^{(i)} \tag{7.10}$$

and, $\mathbf{C}_t^{(i)} = \mathbf{C} \ \forall\, i = 1, 2, 3, \ldots$, derived from the consideration that the bulk, material outside of the discontinuity, remains elastic. Since the second equation in the system (7.4) is complete at elemental level, a partial solution by a static condensation may be performed as

$$d\tilde{\mathbf{u}}^{(i+1)} = \left(\mathbf{K}_{\tilde{u}\tilde{u}}^{(i)}\right)^{-1} \left[\mathbf{R}_{\tilde{u}}^{(i)} - \mathbf{K}_{\hat{u}\tilde{u}}^T d\hat{\mathbf{u}}^{(i+1)}\right] \tag{7.11}$$

which may be substituted into the first equation to obtain

$$\hat{\mathbf{R}}_{\hat{u}}^{(i+1)} = \mathbf{R}_{cond}^{(i)} - \mathbf{K}_{cond}^{(i)} d\hat{\mathbf{u}}^{(i+1)} \tag{7.12}$$

where

$$\mathbf{R}_{cond}^{(i)} = \mathbf{R}_{\hat{u}}^{(i)} - \mathbf{K}_{\hat{u}\tilde{u}} \left(\mathbf{K}_{\tilde{u}\tilde{u}}^{(i)} \right)^{-1} \mathbf{R}_{\tilde{u}}^{(i)} \qquad (7.13)$$

$$\mathbf{K}_{cond}^{(i)} = \mathbf{K}_{\hat{u}\hat{u}} - \mathbf{K}_{\hat{u}\tilde{u}} \left(\mathbf{K}_{\tilde{u}\tilde{u}}^{(i)} \right)^{-1} \mathbf{K}_{\hat{u}\tilde{u}}^{T} \qquad (7.14)$$

The condensed stiffness matrix and internal force vectors of the element are used in the assemblage of the global system of equations. After solving the global system of equations for the incremental displacement $d\hat{\mathbf{u}}^{(i+1)}$, the new nodal displacements are updated

$$\hat{\mathbf{u}}^{(i+1)} = \hat{\mathbf{u}}^{(i)} + d\hat{\mathbf{u}}^{(i+1)} \qquad (7.15)$$

To compute the updated displacement jump $\tilde{\mathbf{u}}^{(i+1)}$, at elemental level, the incremental displacement $d\hat{\mathbf{u}}^{(i+1)}$ has to be substituted back into equation (7.11) to obtain

$$\tilde{\mathbf{u}}^{(i+1)} = \tilde{\mathbf{u}}^{(i)} + d\tilde{\mathbf{u}}^{(i+1)} \qquad (7.16)$$

The advantage of using incompatible modes is that the extra degrees of freedom representing enhanced modes are never considered in the global system of equations. For fracture and strain localization problems where discontinuities are added to relatively few elements compared to the total number of elements, the computational cost involved in solving the extra degrees of freedom is minimal. Also, since the extra degrees of freedom are solved at elemental level, the method can be easily implemented in existing finite element programs. In this work, the numerical implementation of the discrete approach of the adopted embedded discontinuity formulation, has been carried out in the *Finite Element Analysis Program* (FEAP), developed at the University of California at Berkeley by Prof. R. L. Taylor, [108].

7.2 Alternative static condensation

It should be noted that the last steps to compute the incremental displacement jump $d\tilde{\mathbf{u}}^{(i+1)}$, equation (7.11), may not be performed until after the elements matrices are assembled and the resulting global system of equations is solved for the incremental displacement $d\hat{\mathbf{u}}^{(i+1)}$. Consequently, for this algorithm, it is necessary to store the element matrices, for each element with a discontinuity, used in equation (7.11) for the later update of the enhanced modes. This formulation requires additional storage for with respect to that needed for a standard displacement formulation.

It is possible to modify the above algorithm such that only the current values of the enhanced modes parameters are stored. The alternative algorithm is given by linearizing the residual $\mathbf{R}_{\tilde{u}}$ only with respect to $\tilde{\mathbf{u}}$. Accordingly, with $\hat{\mathbf{u}}^{(i)}$ known, the next step is for each element with a discontinuity to compute the displacement jump values $\tilde{\mathbf{u}}^{(i-1)}$ and perform the following steps.

1. For $k = 0$ set

$$\tilde{\mathbf{u}}^{(i,k)} = \tilde{\mathbf{u}}^{(i-1)}$$

   where a single superscript i denotes the value of $\tilde{\mathbf{u}}^{(i)}$ computed in the last global iteration.

2. Compute the linear part of $\mathbf{R}_{\tilde{u}}$ as

$$\mathbf{R}_{\tilde{u}}\left(\hat{\mathbf{u}}^{(i)}, \tilde{\mathbf{u}}^{(i,k)}\right) - \mathbf{K}_{\tilde{u}\tilde{u}}^{(i,k)} d\tilde{\mathbf{u}}^{(i,k+1)} = \mathbf{0}$$

   where now

$$\mathbf{K}_{\tilde{u}\tilde{u}}^{(i,k)} = \int_{\Omega} \mathbf{B}_c^T \mathbf{C} \mathbf{B}_c \, \mathrm{d}\Omega + \int_{\Gamma_d} \mathbf{T}_t^{(i,k)} \, \mathrm{d}\Gamma$$

   with

$$\mathbf{T}_t^{(i,k)} = \left. \frac{\partial \mathbf{t}}{\partial \tilde{\mathbf{u}}} \right|_{\tilde{u}^{(i,k)}}$$

3. Solve for the increment

$$d\tilde{\mathbf{u}}^{(i,k+1)} = \left(\mathbf{K}_{\tilde{u}\tilde{u}}^{(i,k)}\right)^{-1} \mathbf{R}_{\tilde{u}}^{(i,k)}$$

4. Update the solution

$$\tilde{\mathbf{u}}^{(i,k+1)} = \tilde{\mathbf{u}}^{(i,k)} + d\tilde{\mathbf{u}}^{(i,k+1)}$$

5. Set $k \leftarrow k + 1$ and repeat steps 2 to 4 until convergence is achieved, or a predefined maximum number of iterations is reached.

6. Set

$$\tilde{\mathbf{u}}^{(i)} = \tilde{\mathbf{u}}^{(i,k+1)}$$

   and store for the next global iteration.

The only information to be stored is $\tilde{\mathbf{u}}^{(i)}$. The algorithm requires repeated computation of $\mathbf{R}_{\tilde{u}}^{(i,k)}$ and $\mathbf{K}_{\tilde{u}\tilde{u}}^{(i,k)}$. Once the $k-$iteration is completed, linearization with respect to both $\hat{\mathbf{u}}$ and $\tilde{\mathbf{u}}$ is performed, leading to equations (7.12) to (7.14) for the global steps. If convergence is reached at iteration k, the residue $\mathbf{R}_{\tilde{u}}^{(i)}$ in equations (7.12) to (7.14) is zero, thus simplifying slightly the steps involved.

Chapter 8

Numerical examples

This chapter illustrates the numerical simulation of the damage process by means of the *embedded discontinuity* model through two examples. The aim of these examples is to show the numerical and theoretical consistency of the formulation using the small deformation theory, and an state of quasi–static loading. In these examples the damage is simulated by considering only the Mode–I of failure, for quasi–brittle materials, since no shear stresses are allowed along the crack.

There are some aspects to consider, in the analysis procedure, common to both examples. Regarding the solution of the non linear problem, the Standard Newton–Raphson scheme is used together with a displacement control to overcome the peak point of the curve, displacement *versus* load. Furthermore, the discontinuity is introduced perpendicular to the direction of the maximum principal stress, as the Rankine criterion in classical plasticity theory; as soon as this reaches the tensile strength of the material.

8.1 Uniaxial tension test

In this numerical example, the mechanical response of an specimen subjected only to a tension state is analyzed. This problem has been widely studied, with laboratory experiments and numerical models, at the Technical University of Delft, by Van Vliet [111] to get insight into the physical mechanisms underlying the size effect problem in quasi–brittle materials such as concrete and rock.

The dimensions of the specimen and the material parameters, employed in this work, correspond to the final specimen geometry used by Van Vliet, since at the beginning of his research he tried different geometries before obtaining an specimen which guaranteed the desired pure tension state in the the entire solid. In this work only the concrete test (I), of the DRY series, specimens were stored directly in the laboratory without any special care, is studied. The geometry, corresponding to specimen denominated "type C", is shown in figure 8.1; where the characteristic dimension D was taken as $200mm$, radius $r = 145mm$, and depth $= 100mm$. As for the geometry dimensions, the material properties were taken
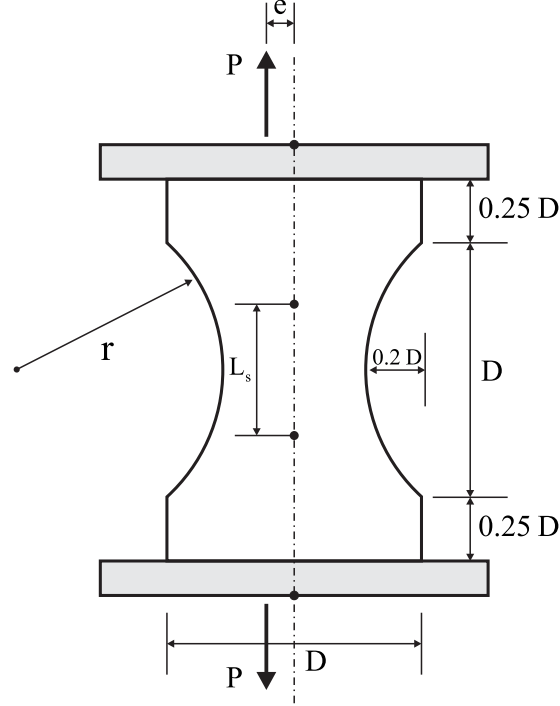
Figure 8.1: Plate subjected to a load P applied with an eccentricity e.

as an average of those reported in the laboratory experiments, for the type of specimen used (05C04N30). Elastic modulus $E = 39.8GPa$, Poisson ratio $\nu = 0.2$, tensile strength $\sigma_{t0} = 2.57MPa$ and fracture energy $G_F = 0.1219\frac{N}{mm}$.

To assure an uniform transference of the load on the top and bottom parts of the specimen, two steel plates were introduced in the laboratory experiments; allowing a free rotation. In the numerical simulation, this condition was reproduced through two layers of elements with material properties corresponding to the steel employed in the test; avoiding the effect of load concentration when this is applied at a discrete point, characteristic of the FEM. Regarding the application of loading, to guarantee a tensile state of stress in the entire cross section, a load eccentricity was introduced according to the theory of linear elasticity [111], $e = \frac{D}{50}(mm)$; allowing a free rotation of the layers, shown in figure 8.1.

In the laboratory experiments the specimen was fully instrumented, by means of LVDTs (Linear Variable Displacement Transducer), to obtain the deformation over the middle cross section of the specimen. In the present numerical simulation, only the deformation along the vertical axis is considered for the comparison of results. Figure 8.1 shows the reference points, chosen to obtain the deformation, which initially were separated a distance $L_s = 0.6D$.

Regarding the discretization of the domain, by the finite element method, an structured mesh with constant strain triangles and a plane stress state is employed; where the crack pattern was prescribed, taking into account the symmetry of the geometry and boundary conditions used in the laboratory tests, figure 8.2. The aim of using this mesh, with
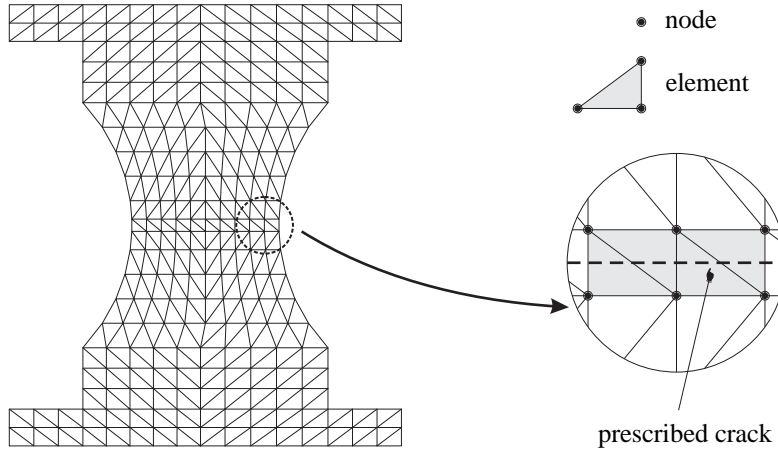
Figure 8.2: Mesh using triangular elements, structured mesh.

a prescribed crack pattern, is to validate the application of the embedded discontinuity formulation to problems where the propagation of the crack is already known. However, this does not invalidate the application of the formulation to problems where the crack patter is unknown. This is due to the fact that the main application of this numerical model is in the simulation of crack growth starting from a state without cracks in the solid; eliminating the remeshing process necessary when *interface elements* are used to propagate the crack.

In figure 8.3 the curve deformation *versus* load is shown. The deformation is computed as the relative displacement between the points originally separated a distance L_s, measured in micrometers μm $(1\mu\text{m} = 10^{-6}\text{m})$. Two numerical responses are plotted attending to the used softening law; the continuous thin line corresponds to the linear softening whereas the continuous thick line is for the exponential. The experimental results are plotted as a dotted line. In this figure it is observed that the elastic branch is correctly reproduced by the numerical simulation, for both softening laws, until the peak load. The differece between the maximum experimental load and that obtained by the numerical simulation is, as an average, 1% lower for the numerical results. This fact is due to the cohesive zone model used, developed in chapter 3, which considers that the Mode–II occurs together with the Mode–I in brittle form, without energy dissipation [87]. The used stiffness for this mode is taken equal to zero.

In general, the simulation response is correctly reproduced by the numerical model. However, from the experimental unloading branch which shows a response partially ductile, the best approximation of the global behavior is obtained with the exponential softening law because this gives a better energy dissipation; fact reflected in a better ductility in the model. This may be explained as follows. In the first part of this branch the exponential softening law dissipates energy faster than the linear softening, while in the final part the opposite happens.

With respect to the assumption made in the formulation above, the rigid body motion
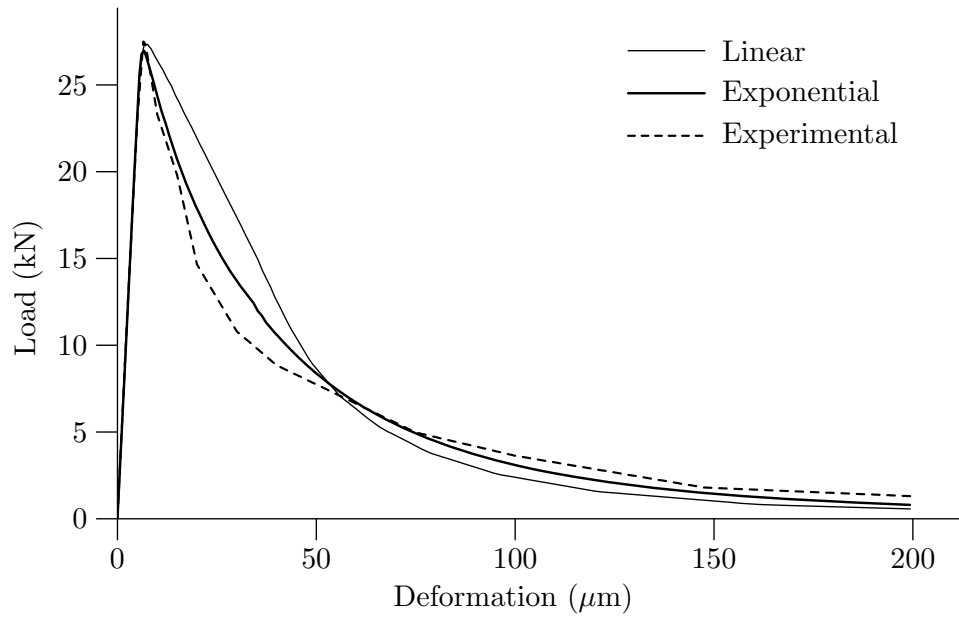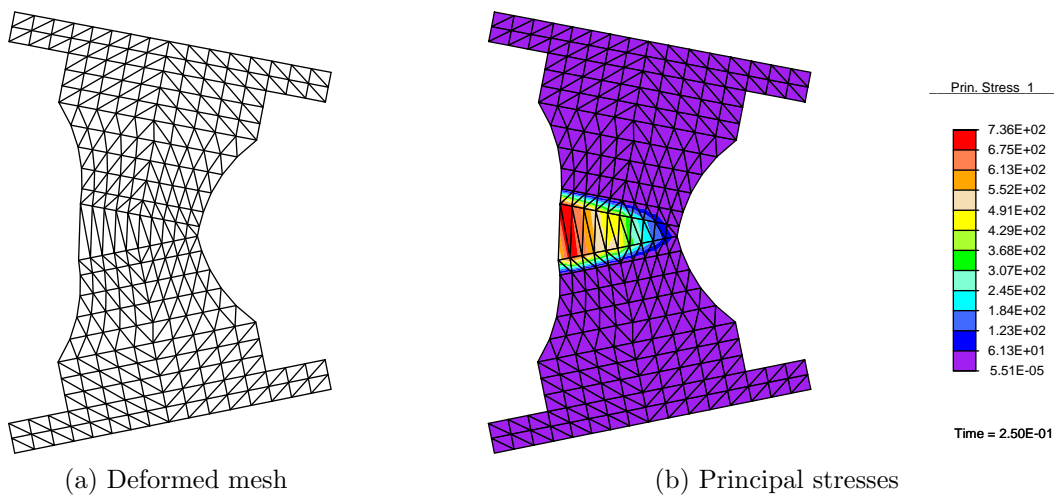
Figure 8.3: Global response of the specimen.

(a) Deformed mesh

(b) Principal stresses

Figure 8.4: Deformed mesh showing a rigid body motion of the solid divided by Γ_d.

of the two parts in which the solid is divided; this can be observed in figure 8.4. The deformed mesh is shown in figure 8.4a where the elements located at the middle part are completly crossed by the crack; whereas the others which belong to the bulk do not undergo any distortion in their geometry. Similarly in figure 8.4b, the maximum principal stresses σ_I are plotted. Here, it is clear that the two parts in which the solid is divided by the crack unload elastically without energy dissipation and that only the elements located in the middle part of the solid dissipate energy in accordance to the cohesive model, see chapter 3; assuring a rigid body motion.

From this example it may be concluded that:

- The employed material parameters were properly taken from the experimental report [111]. This is reflected in the shape of the numerical simulation curve where the peak load is almost equal to that obtained in the laboratory tests. Furthermore, the ductile behavior of the numerical curve for the exponential softening law, is very similar to the obtained experimentally.

- The elastic branch of curve in figure 8.3 is equal to the experimental. It is important to point out that this result is only possible when the boundary conditions are the same, in the numerical simulation and in the experimental tests.

- In general, the embedded discontinuity formulation, developed in this work, is able to simulate numerically problems where the crack pattern is known in advance, with a consistent energy dissipation.

8.2   Single notched four points beam

The four–point–shear tests simulated by many authors using: continuum models [56, 83, 93], the embedded discontinuity method [26, 41, 94, 95], and meshless methods [48, 84], is addressed in this section. Since the pioneer experimental work of Arrea and Ingraffea [10], this type of experiments have been widely used to study the damage process under a mixed mode of failure. Similar laboratory tests have been carried out by Schlangen [97, 98] and others.

For quasi–brittle materials such as concrete, the fracture is still locally driven by the maximum tensile stress [56]. This four–points–shear problem undergoes a tension–compression state which gives rise to a curved propagation of the crack, starting from the notch tip in an inclined direction.

Figure 8.5 illustrates the loading system applied to the beam which is antisymmetric and leads to a cracking failure dominated by Mode–I of fracture. The material properties and the geometry of the problem were taken from the work of Schlangen [98].

The geometry of the beam is shown in figure 8.5 with its dimensions in millimeters; the depth is of $100mm$. The beam has at the top of the symmetry axis a $5mm$ wide, a
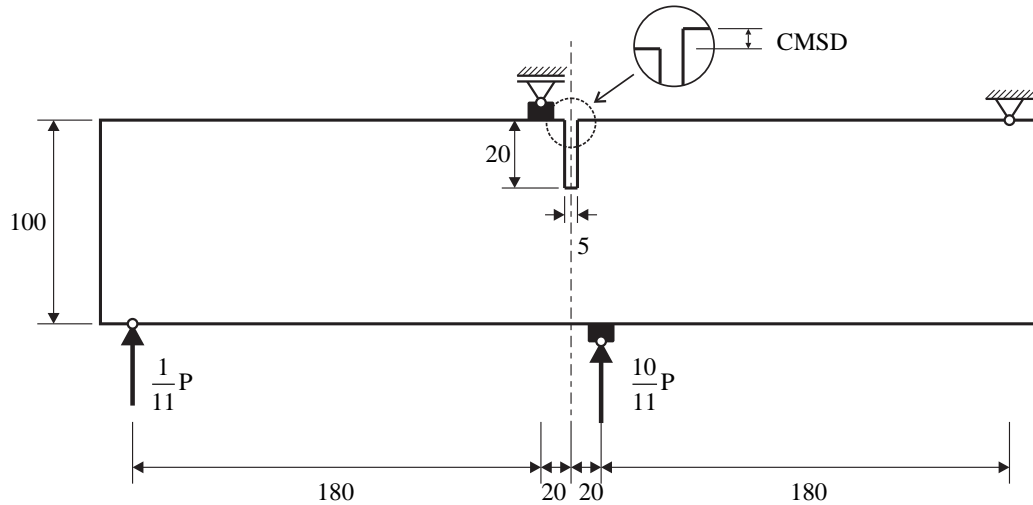
Figure 8.5: Single–notched four points beam
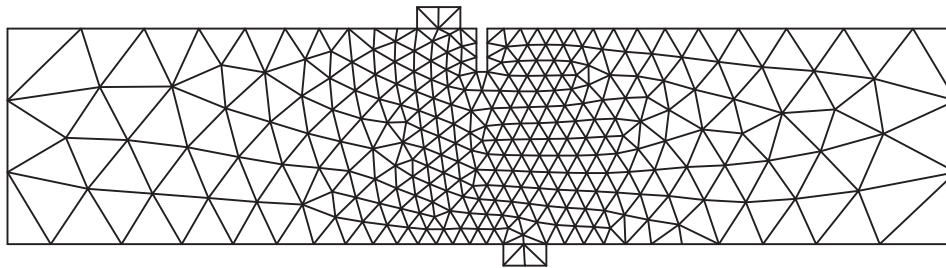
Figure 8.6: Discretization of the single notched four points beam by the FEM

$20mm$ deep notch. All relevant dimensions of the beam and its supports at the top and bottom are shown in the figure. As for the uniaxial tension test example, the material properties were taken only for one series of the laboratory experiments, beam type SEN. The material data are as follows: Young's modulus $E = 30GPa$, Poisson ratio $\nu = 0.20$, two tensile strengths are considered, $\sigma_{t0} = 2.8MPa$ and $\sigma_{t0} = 3.0MPa$, and fracture energy of $G_F = 0.10\frac{N}{mm}$.

To reproduce the experimental results reported by Schlangen, in the numerical simulation the *sliding displacement of the crack mouth* (CMSD) was measured; which is the relative vertical displacement between the tow sides of the notch, see figure 8.6. The support on the left side has its vertical displacement restricted whereas the other, located at the right side, has fixed both directions.

For the simulation of damage, the discrete damage model presented in chapter 3 is used. In this model, shear effects are neglected and the crack grows according to the Rankine criterion, *i.e.,* when the maximum principal stress reaches the tensile strength of the material.

Constant strain triangles are used in the discretization with finite elements. The non–

Figure 8.7: Load P *versus* CMSD of the single notched four point beam

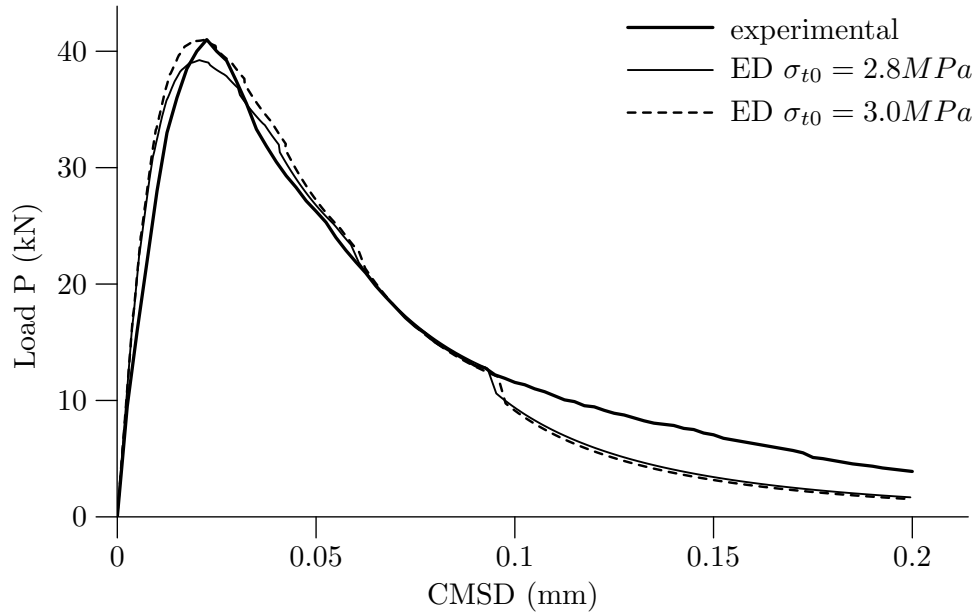structured mesh is shown in figure 8.6. The analyses are carried out using a plane stress formulation. At the points of load application, additional elements were included to obtain a better distribution of loading at these points, similar to the laboratory experiments where steel plates were placed.

Unlike the first example, where the crack pattern was prescribed, in this problem the crack propagation is not *a priori* enforced, and its path is determined by the direction of the maximum principal stress, *i.e.,* the crack is introduced perpendicular to the σ_I direction. This way of introducing the crack pattern, without knowing in advance the crack trajectory, makes the embedded discontinuity formulation very promising in problems where the crack propagation across the continuum is needed. Furthermore the mesh modification used when discrete elements are employed is eliminated, since the crack can cross the elements in the embedded discontinuity formulation.

The numerical response, load *versus* CMSD, is shown in figure 8.7. The curve corresponding to the experimental test is plotted in continuous thick line and for the numerical simulations, using an exponential softening law, two curves are presented: the first one with a strength of $\sigma_{t0} = 2.8MPa$ is plotted in continuous thin line whereas the dotted line corresponds to a strength of $\sigma_{t0} = 3.0MPa$. In this figure it may be observed that the loading branches for both numerical simulations are almost the same with the only difference in the peak load; the higher corresponding to the strength $\sigma_{t0} = 3.0MPa$, as it was expected.

With respect to the experimental results, in the same branch, it is observed that the numerical response coincides only until about $P = 10kN$, likely when the linear elastic behavior ends, and from this point the response is different. This situation may be attributed to: in
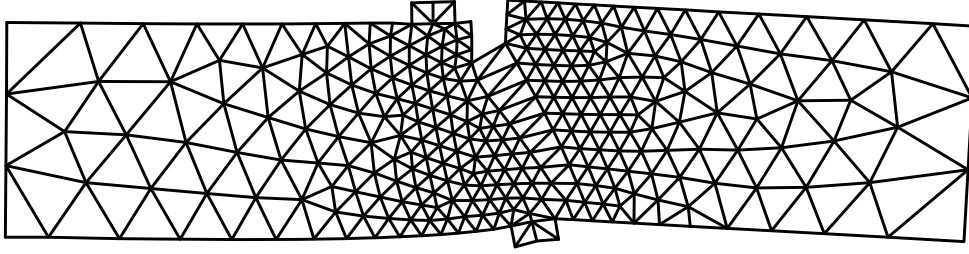
Figure 8.8: Deformed mesh obtained for the single notched four points beam

lower grade to the employed material properties in the numerical simulation, and second to the important influence of the modeling of the supports used in the experiments. In the simulation different support systems were considered. In each case the response was strongly influenced by the support system.

Regarding the unloading branch, it is observed that the numerical and experimental curves are almost equal until a CMSD of $0.1mm$ where there is a rapid descend in the numerical response attributable to the lack in the computed crack propagation, maximum principal stress criterion, when an isotropic damage model is used. This problem rises when the crack reaches the last elements located in the bottom part of the beam, leading to an hydrostatic stress state. Despite of this it is important to point out that the numerical simulation reproduces with a good accuracy the global response of the solid, especially the ductile behavior of the material.

In figure 8.8 the deformed mesh is shown. In this figure it may be observed that the crack pattern is curved where the inelastic response is located; while the bulk unloads elastically. A zoom to the center of the beam where the crack propagates is shown in figure 8.9. The crack pattern which is not *a priori* enforced is plotted with continuous thick line. Since all the intra–element cracks are forced to pass through the centroid of the elements, the experimental crack pattern can not be accurately reproduced. To improve this, it is necessary to enforce the crack path continuity across the elements together with a finer mesh.
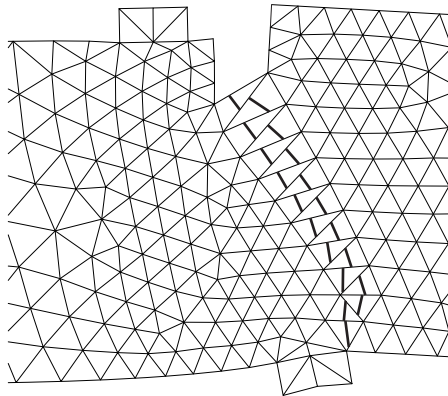
Figure 8.9: Crack pattern across the elements
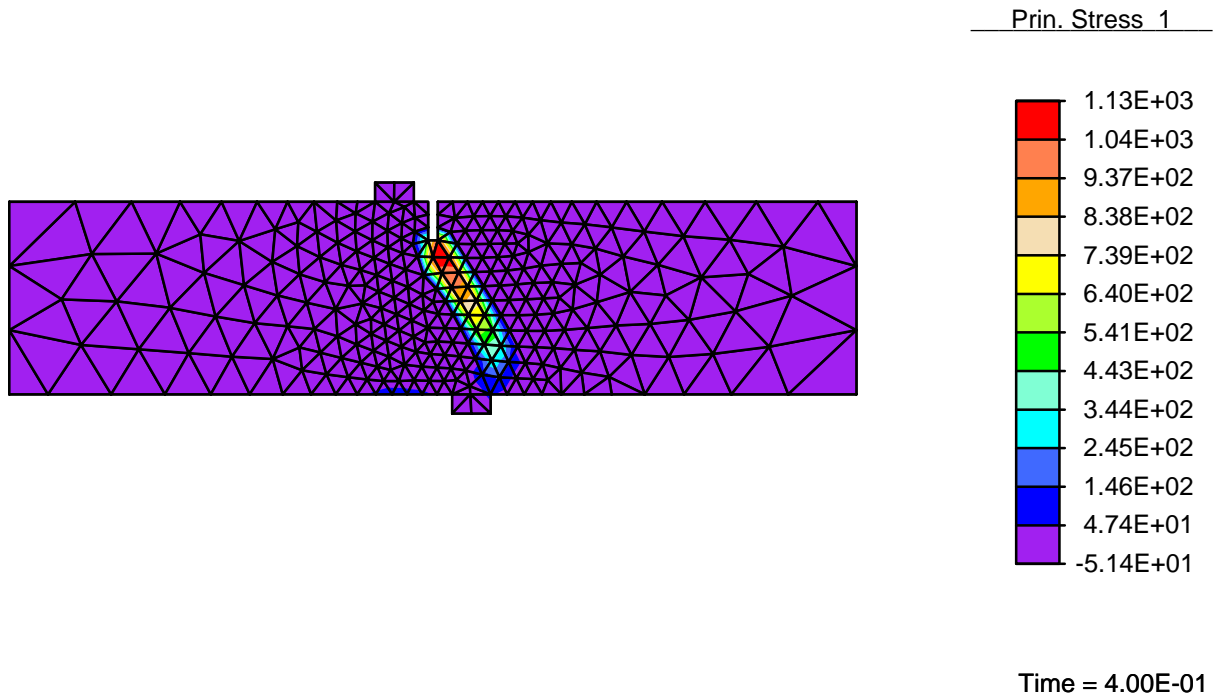
Figure 8.10: Maximum principal stresses showing unloading of the bulk

Finally, in figure 8.10 the maximum principal stresses σ_I are plotted. In this figure it is observed that the maximum values of the stresses occurs in the elements located in the crack pattern while those in the bulk undergo a linear elastic unloading process; giving a rigid body motion of the two parts in which the continuum is divided by the macro crack.

Some important issues from this example, related with the support system used and the material properties employed, are summarized in what follows:

- As it was mentioned above, the support system is highly important since if it does not represent satisfactory the system used in the laboratory tests, even the branch corresponding to the elastic response of the problem is not correctly reproduced in numerical simulation.

- A possible explanation to the difference between the numerical and experimental curves may be due to the uncertainty in the measured material properties in the experimental tests.

- An other possible reason is that, in the best knowledge of the author, is related with the employed cohesive model. To improve the numerical response it may be necessary to use a material model which considers the mixed Mode of failure, I–II, and a model with non–isotropic damage behavior.

Chapter 9

Conclusions

In this thesis the symmetric embedded discontinuity model, used to numerically simulate the damage process in quasi–brittle materials, is formulated within a consistent variational framework starting from the general variational formulation of VHW, valid for a continuum solid, and after a generalization of it for a solid with discontinuities. In the variational formulation the effect of the discontinuity is introduced in the energy functional as an additional term, which considers the energy dissipated in the discontinuity boundary. From the variational formulation it is shown that all the field equations, stationary conditions of the functional, which govern the associated *Boundary Value Problem* are obtained in a natural way. It is shown that the traction equilibrium across the discontinuity Γ_d is derived naturally; unlike the non–symmetric formulation which introduces this condition by modifying the governing equations of the problem. However, when the FEM is used to approximate the system of differential equations, the traction continuity is not imposed properly when the crack band collapses into a line, discrete approach. To eliminate the drawback of this approach, the traction continuity is enforced by introducing an additional variable in the discrete form of the problem.

In chapter 6, it is demonstrated that the geometry of the discontinuity influences the numerical response. This geometric condition leads to a specific surface where the equilibrium, across the discontinuity, has to be evaluated.

Regarding the numerical implementation of the embedded discontinuity formulation, when an elemental enhancement without path continuity is used, a tracking algorithm has to be consider to obtain a satisfactory response. Otherwise a chaotic crack growth may be produced in the entire continuum since cracks are allowed to develop in any element with not path continuity. In this work only one crack located at the centroid of the element is allowed to develop. Furthermore, the only possible element to undergo damage is that located in front of the crack tip. This may seem a restrictive procedure but as it is shown to give good results. In this way only one crack dissipates energy.

The cohesive zone model, is used as material model to simulate the damage process in a discontinuity surface which considers that the global behavior is governed by two material properties; the tensile strength σ_{t0} and the fracture energy G_F. In this model, the energy

dissipation due to the Mode–II of failure is neglected since it is assumed that the response is dominated by the Mode–I of material failure. Strictly speaking this considerations lead to a scalar damage model. The discontinuity is introduced, at elemental level, perpendicular to the direction of the maximum principal stress σ_I when this reaches the tensile strength of the material, similar to the Rankine criterion in classical plasticity theory.

The validity of the adopted embedded discontinuity formulation, discrete approach, is evaluated by means of two numerical examples presented in chapter 8. The first example is a simple tension specimen which has been studied in experimental tests. Particularly in the numerical simulation of this problem, the crack pattern is *a priori* prescribed, taking advantage of the geometry and boundary conditions of the experimental test, and the numerical results are compared with those reported by the laboratory tests. It is found that the experimental response of the specimen is satisfactorily modeled by means of the embedded discontinuity formulation. The best softening law, for this problem, is the exponential since it is able to dissipate energy with a relative degree of ductility, as it happens in the laboratory experiments.

The second example is a four–point–beam with a single notched at its upper part. In this problem only the Mode–I of failure is considered. This may be a poor numerical simulation of the experimental tests since the aim of this problem is to study the influence of the mixed Mode, I–II. However the objective in the modeling of the problem, in this work, is to evaluate the numerical consistency of the presented embedded discontinuity model leaving the solution of actual practical problem for a later future. Despite that only the Mode–I has been considered, it is shown that the numerical simulation reproduce, with a good accuracy, the results of laboratory experiments.

In general it is shown that the symmetric embedded discontinuity formulation is able to give robust results when the traction equilibrium, across the discontinuity, is evaluated in a specific surface. This gives rise to a *strong* traction continuity.

In order to improve the numerical results, it may be important to consider constitutive models where the effect of the Mode–II is taken into account, in a coupled or uncoupled form, together with the Mode–I. Additionally, the crack path continuity should be enforced across element to guarantee a best energy dissipation.

Appendix A

Tensors and notations

The analysis of an engineering system requires its idealization into a form that can be solved numerically. The use of tensors in engineering analysis is of fundamental importance because it is by using these quantities that the complete solution process can be expressed in a compact and elegant manner.

The main objective of this appendix is to present, in a compact form, the fundamentals of tensor algebra and the different notations commonly employed in engineering: matrix, indicial, tensorial and voigt notations; with emphasis on those aspects that are important for the formulation of finite element analysis and its numerical implementation, [19, 25, 43, 50, 63, 71, 96, 118].

A.1   Indicial notation

This notation, which is also called component notation, uses indexed components along with abbreviation rules such as commas for partial derivatives and Einstein's summation convention. It is a powerful notation, and as such is preferred in journals and monographs. It has the advantage of readily handling arbitrary tensors of any order, arbitrary coordinate systems and nonlinear relations. It sharply distinguishes between covariant and contravariant quantities, which is necessary in non–Cartesian coordinates. However, it tends to conceal or mask intrinsic properties, and as such it is not suitable for basic instruction.

Consider a point $P(x_1, x_2, x_3)$ in Cartesian coordinate system, figure A.1, which may be represented by the compact notation

$$P(x_i) \qquad i = 1, 2, 3 \tag{A.1}$$

where x_i means x_1, x_2, x_3.
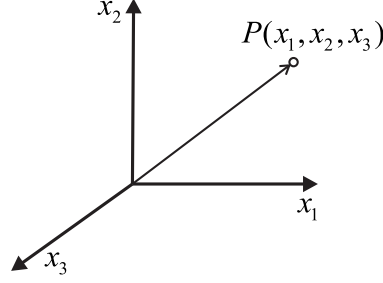
Figure A.1: Point P in a rectangular Cartesian coordinate system.

A linear algebraic set of equations involving the Cartesian coordinates (x_1, x_2, x_3) is ordinarily written using the summation operator as

$$\sum_{j=1}^{3} a_{ij}x_j = b_i \qquad i = 1, 2, 3 \tag{A.2}$$

where a_{ij} and b_i are constants. This expands to three equations:

$$i = 1: \quad \sum_{j=1}^{3} a_{1j}x_j = b_1, \quad \text{or} \quad a_{11}x_1 + a_{12}x_2 + a_{13}x_3 = b_1,$$

$$i = 2: \quad \sum_{j=1}^{3} a_{2j}x_j = b_2, \quad \text{or} \quad a_{21}x_1 + a_{22}x_2 + a_{23}x_3 = b_2, \tag{A.3}$$

$$i = 3: \quad \sum_{j=1}^{3} a_{3j}x_j = b_3, \quad \text{or} \quad a_{31}x_1 + a_{32}x_2 + a_{33}x_3 = b_3,$$

and in an even shorter notation as

$$a_{ij}x_j = b_i \tag{A.4}$$

in which the summation symbol has been suppressed. This is the *summation convention*, *i.e.*, an index repeated in an expression is understood to be summed over the implied range. In three–dimensional continuum mechanics, the range is from 1 to 3.

In an expression such as

$$a_{ij}x_j \tag{A.5}$$

i is said to be the *free index* which *can* take any of the values $1, 2$ or 3, whereas j is said to be the *dummy index* which *must* take the values $1, 2$ and 3. In other words, the dummy index is the one that must be summed over its entire range.

A.2 Cartesian tensors

In engineering, the concept of tensors and their matrix representations is an important point to consider. Here the presentation will be limited to tensors in a three–dimensional Euclidean space with the representation of tensors in rectangular Cartesian coordinates.

Variables used in engineering mechanics usually have the character of tensors. In general we denote zero–dimensional tensors (scalars) by Latin letters or Greek symbols first–order tensors (vectors) by lowercase Latin letters, second–order tensors by lowercase Greek or Latin letters, and fourth–order tensors by capital Latin letters.

Boldface letters represent the entire the tensors (*compact notation*). When referring to the Cartesian components of tensors (*indicial notation*) we use lowercase Latin subscripts $i, j, k, l, \ldots$, which can take values 1, 2 and 3 corresponding to the Cartesian coordinate axes x_1, x_2, and x_3. For example:

$$u_i : \begin{bmatrix} u_1 \\ u_2 \\ u_3 \end{bmatrix}, \quad b_i : \begin{bmatrix} b_1 \\ b_2 \\ b_3 \end{bmatrix}, \quad t_i : \begin{bmatrix} t_1 \\ t_2 \\ t_3 \end{bmatrix} \qquad \text{for } i = 1, 2, 3 \tag{A.6}$$

identify the vectors of displacements, body forces and surface tractions, respectively. All these quantities are first–order tensors. Others tensors, widely used in elasticity are the, second–order, strain and stress tensors stated as

$$\varepsilon_{ij} : \begin{bmatrix} \varepsilon_{11} & \varepsilon_{12} & \varepsilon_{13} \\ \varepsilon_{21} & \varepsilon_{22} & \varepsilon_{23} \\ \varepsilon_{31} & \varepsilon_{32} & \varepsilon_{33} \end{bmatrix}, \quad \sigma_{ij} : \begin{bmatrix} \sigma_{11} & \sigma_{12} & \sigma_{13} \\ \sigma_{21} & \sigma_{22} & \sigma_{23} \\ \sigma_{31} & \sigma_{32} & \sigma_{33} \end{bmatrix} \qquad \text{for } \begin{cases} i = 1, 2, 3 \\ j = 1, 2, 3 \end{cases} \tag{A.7}$$

To define the constitutive tensor, operator relating strains with stresses, a fourth–order tensor is employed as

$$D_{ijkl} : \begin{bmatrix} \left\{ \begin{matrix} D_{1111} & D_{1112} & D_{1113} \\ D_{1121} & D_{1122} & D_{1123} \\ D_{1131} & D_{1132} & D_{1133} \end{matrix} \right\} & D_{12kl} & D_{13kl} \\ & & \\ & D_{21kl} & D_{22kl} & D_{23kl} \\ & D_{31kl} & D_{32kl} & D_{33kl} \end{bmatrix} \qquad \text{for } \begin{cases} i = 1, 2, 3 \\ j = 1, 2, 3 \\ k = 1, 2, 3 \\ l = 1, 2, 3 \end{cases} \tag{A.8}$$

In equation (A.8), for simplicity, only the submatrix D_{11kl} has been expanded; the rest of the terms can be expanded in same form. This fourth–order tensor has $3^4 = 81$ terms.

A.3 Tensorial notation

In this type of notation, the indices are not shown. While indicial notation only apply to Cartesian coordinates, expressions in tensor notation are independent of the coordinate system and apply to other coordinate such as cylindrical, curvilinear, etc. Furthermore, equations in tensor notation are easier to memorize. A large part of continuum mechanics and finite element literature employs tensor notation.

Tensors of order one or greater are indicated in boldface. Lower case boldface letters are almost used for first–order tensors, while upper case boldface letters are used for higher–order tensors. For example, the velocity vector is $\mathbf{v}$ in tensor notation, while a second–order tensor, such as $\mathbf{E}$, is written in upper case. The major exception is the Cauchy stress tensor $\boldsymbol{\sigma}$, which is denoted by a lower case symbol.

For example equation (A.2) is written in tensor notation as

$$\mathbf{A} \cdot \mathbf{x} = \mathbf{b} \tag{A.9}$$

where a dot denotes contraction of the inner indices; in this case, the first tensor is of second order the second term is of first order; hence the resultant tensor is of first order since there is a contraction of one index.

Tensor expressions are distinguished from matrix notation by using dots and colons between terms, as in $\mathbf{A} \cdot \mathbf{x}$. The symbol ':' denotes the contraction of a pair of repeated indices which appear in the same order, so $\mathbf{A} : \mathbf{B} = A_{ij}B_{ij}$. As another example, a linear constitutive equation is given below in tensor notation and indicial notation

$$\sigma_{ij} = C_{ijkl}\varepsilon_{kl} \qquad \boldsymbol{\sigma} = \mathbf{C} : \boldsymbol{\varepsilon} \tag{A.10}$$

A.4 Matrix notation

The matrix notation was invented primarily to express linear algebra relations in compact form. Compactness enhances visualization and understanding of essentials. The matrix notation is similar to the previous one, but entities are rearranged as appropriate so that only matrix operations are used. The main advantages of matrix notation are historical compatibility with finite element formulations, and ready computer implementation in symbolic or numeric form. Examples of column matrices are

$$\mathbf{x} : \begin{Bmatrix} x \\ y \\ z \end{Bmatrix}, \qquad \mathbf{v} : \begin{Bmatrix} v_1 \\ v_2 \\ v_3 \end{Bmatrix} \tag{A.11}$$

Usually rectangular matrices will be denoted by upper case boldface, such as $\mathbf{A}$, The transpose of a matrix is denoted by a superscript T, and the first index always refers to a row number, the second to a column number. Thus a 2×2 matrix $\mathbf{A}$ and a 2×3 matrix $\mathbf{B}$ are written as follows

$$\mathbf{A} : \begin{bmatrix} A_{11} & A_{12} \\ A_{21} & A_{22} \end{bmatrix}, \qquad \mathbf{B} : \begin{bmatrix} B_{11} & B_{12} & B_{13} \\ B_{21} & B_{22} & B_{23} \end{bmatrix} \tag{A.12}$$

The representation of scalars, which may be viewed as 1×1 matrices, does not change, the same as the representation of vectors because vectors are column (or row) matrices.

A.5   Voigt notation

In finite element implementations, symmetric second–order tensors are often written as column matrices. This and any other conversion of higher–order tensors to column matrices use the *Voigt notation*. The procedure to convert symmetric second–order tensors to column matrices is called the Voigt rule. For a detailed description of this notation, the reader is referred to the book of Belytschko *et al.* [19].

Two–dimensional symmetric tensors are converted to one–dimensional arrays that list only the independent components (six in three dimensions, three in two dimensions). Component order is a matter of convention, but usually the diagonal components are listed first, followed by the off–diagonal components.

For the strain and stress tensors this vectorization process produces the vectors

$$\{\boldsymbol{\varepsilon}\} : \begin{bmatrix} \varepsilon_{11} \\ \varepsilon_{22} \\ \varepsilon_{33} \\ \varepsilon_{23} \\ \varepsilon_{13} \\ \varepsilon_{12} \end{bmatrix}, \qquad \{\boldsymbol{\sigma}\} : \begin{bmatrix} \sigma_{11} \\ \sigma_{22} \\ \sigma_{33} \\ \sigma_{23} \\ \sigma_{13} \\ \sigma_{12} \end{bmatrix} \tag{A.13}$$

In view of equations (A.13), the fourth–order constitutive tensor C_{ijkl} has to be mapped into a second–order tensor C_{ij} to agree with, this index changing may be developed according to table A.1.

The transformation indices are: $C_{1111} \rightarrow C_{11}$; $C_{2233} \rightarrow C_{23}$; $C_{1231} \rightarrow C_{46}$; etc. The final mapping of the fourth–order tensor to one of second–order is shown in equation (A.14)

Form	Index number					
	1	2	3	4	5	6
Matrix	1	2	3	4	5	6
Tensor	11	22	33	12 & 21	23 & 32	31 & 13

Table A.1: Mapping between matrix and tensor indices

$$C_{ij} : [C] : \begin{bmatrix} C_{11} & C_{12} & C_{13} & C_{14} & C_{15} & C_{16} \\ & C_{22} & C_{23} & C_{24} & C_{25} & C_{26} \\ & & C_{33} & C_{34} & C_{35} & C_{36} \\ & & & C_{44} & C_{45} & C_{46} \\ & sym. & & & C_{55} & C_{56} \\ & & & & & C_{66} \end{bmatrix} \tag{A.14}$$

For example, the linear elastic law in indicial notation involves the four–order tensor C_{ijkl}

$$\sigma_{ij} = C_{ijkl}\varepsilon_{kl} \quad \text{or in tensor notation} \quad \boldsymbol{\sigma} = \mathbf{C} : \boldsymbol{\varepsilon} \tag{A.15}$$

The Voigt matrix form of the above is

$$\{\boldsymbol{\sigma}\} = [\mathbf{C}]\{\boldsymbol{\varepsilon}\} \tag{A.16}$$

A.6 Full notation

In the full form notation every term is spelled out. No ambiguities of interpretation can arise; consequently this works well as a notation of last resort, and also as a comparison template against one can check out the meaning of more compact expressions. It is also useful for programming in low–order languages.

As an example, consider the well known dot product between two physical vectors in 3D space, $a : (a_1, a_2, a_3)$ and $b : (b_1, b_2, b_3)$ done in the four different notations:

$$\underbrace{a_i b_i}_{indicial} : \underbrace{\mathbf{a} \cdot \mathbf{b}}_{tensorial} : \underbrace{\mathbf{a}^T \mathbf{b}}_{matrix} : \underbrace{a_1 b_1 + a_2 b_2 + a_3 b_3}_{full} \tag{A.17}$$

A.7 Basic operations in tensor algebra

In this section, some basic operations between tensor of equal or different orders are reviewed. In what follows, by agreement, scalars will be called a zero–order tensors and

vectors, first–order tensors. Commonly in engineering a second–order tensors is referred as a matrix; these names are used on the understanding that they are tensors.

The dot product or scalar product of two vectors, which produces a scalar, is defined as:

$$\underbrace{u_i v_i}_{indicial} \; : \; \underbrace{\mathbf{u} \cdot \mathbf{v}}_{tensorial} \; : \; \underbrace{\mathbf{u}^T \mathbf{v}}_{matrix} \tag{A.18}$$

The double–dot product of two second–order tensors, which also produces an scalar,

$$\underbrace{\sigma_{ij} \varepsilon_{ij}}_{indicial} \; : \; \underbrace{\boldsymbol{\sigma} : \boldsymbol{\varepsilon}}_{tensorial} \; : \; \underbrace{\boldsymbol{\sigma} \boldsymbol{\varepsilon}}_{matrix} \tag{A.19}$$

The dot product of two second–order tensors, which produces a second–order tensor,

$$\underbrace{\sigma_{ij} \varepsilon_{jk}}_{indicial} \; : \; \underbrace{\boldsymbol{\sigma} \cdot \boldsymbol{\varepsilon}}_{tensorial} \; : \; \underbrace{\boldsymbol{\sigma} \boldsymbol{\varepsilon}}_{matrix} \tag{A.20}$$

Appendix B

The divergence theorem

The way to transform one integral defined over a volume to other on the boundary is by means of the *divergence theorem*, more commonly known, especially in older literature, as *Gauss's theorem* [7], and also known as the *Gauss–Ostrogradsky theorem*. In this appendix, unlike the rest of the thesis, the tensor notation is employed which objective is to show the application of this notation.

The theorem of the divergence is a theorem in vector calculus that can be stated as follows. Let the vector $\mathbf{a}$ and its first derivatives be continuous over the simply connected region of interest. Then the divergence theorem states that

$$\int_\Omega \boldsymbol{\nabla} \cdot \mathbf{a} \, \mathrm{d}\Omega = \int_\Gamma \mathbf{a} \cdot \boldsymbol{\nu} \, \mathrm{d}\Gamma \tag{B.1}$$

In words, the surface integral of a vector $\mathbf{a}$ over a closed surface Γ equals the volume integral of the divergence of that vector integrated over the volume Ω enclosed by the surface Γ.

For the special case of elasticity problems [40], the divergence theorem is applied as follows. Take $\mathbf{a} = \boldsymbol{\sigma} \cdot \mathbf{u}$, where $\boldsymbol{\sigma}$ is a symmetric stress tensor and $\mathbf{u}$ a displacement vector

$$\int_\Omega \boldsymbol{\nabla} \cdot (\boldsymbol{\sigma} \cdot \mathbf{u}) \, \mathrm{d}\Omega = \int_\Gamma (\boldsymbol{\sigma} \cdot \mathbf{u}) \cdot \boldsymbol{\nu} \, \mathrm{d}\Gamma \tag{B.2}$$

where $\boldsymbol{\nabla}$ is the nabla operator, vector, defined as

$$\boldsymbol{\nabla} = \begin{bmatrix} \frac{\partial}{\partial x_1} \\ \frac{\partial}{\partial x_2} \\ \frac{\partial}{\partial x_3} \end{bmatrix} \tag{B.3}$$

Applying nabla to a vector via the dot product yields the divergence of the vector, which is an scalar

$$\boldsymbol{\nabla} \cdot \mathbf{u} = \mathbf{div}\ \mathbf{u} = u_{i,i} = \sum_{i=1}^{3} \frac{\partial u_i}{\partial x_i} = \frac{\partial u_1}{\partial x_1} + \frac{\partial u_2}{\partial x_2} + \frac{\partial u_3}{\partial x_3} \tag{B.4}$$

As for the above case, the application of nabla to a second order tensor yields the divergence of the tensor, the result is a vector

$$\boldsymbol{\nabla} \cdot \boldsymbol{\sigma} = \mathbf{div}\ \boldsymbol{\sigma} = \sigma_{ij,j} = \sum_{j=1}^{3} \frac{\partial \sigma_{ij}}{\partial x_j} = \begin{bmatrix} \frac{\partial \sigma_{11}}{\partial x_1} + \frac{\partial \sigma_{12}}{\partial x_2} + \frac{\partial \sigma_{13}}{\partial x_3} \\ \frac{\partial \sigma_{21}}{\partial x_1} + \frac{\partial \sigma_{22}}{\partial x_2} + \frac{\partial \sigma_{23}}{\partial x_3} \\ \frac{\partial \sigma_{31}}{\partial x_1} + \frac{\partial \sigma_{32}}{\partial x_2} + \frac{\partial \sigma_{33}}{\partial x_3} \end{bmatrix} \tag{B.5}$$

Now the term in the left hand side integral of equation (B.2) may be expanded, considering equations (B.4) and (B.5), as

$$\boldsymbol{\nabla} \cdot (\boldsymbol{\sigma} \cdot \mathbf{u}) = \frac{\partial}{\partial x_1} (\sigma_{11} u_1 + \sigma_{12} u_2 + \sigma_{13} u_3) + \frac{\partial}{\partial x_2} (\sigma_{21} u_1 + \sigma_{22} u_2 + \sigma_{23} u_3) +$$

$$\frac{\partial}{\partial x_3} (\sigma_{31} u_1 + \sigma_{32} u_2 + \sigma_{33} u_3)$$

$$\boldsymbol{\nabla} \cdot (\boldsymbol{\sigma} \cdot \mathbf{u}) = \frac{\partial \sigma_{11}}{\partial x_1} u_1 + \sigma_{11} \frac{\partial u_1}{\partial x_1} + \frac{\partial \sigma_{12}}{\partial x_1} u_2 + \sigma_{12} \frac{\partial u_2}{\partial x_1} + \frac{\partial \sigma_{13}}{\partial x_1} u_3 + \sigma_{13} \frac{\partial u_3}{\partial x_1} +$$

$$\frac{\partial \sigma_{21}}{\partial x_2} u_1 + \sigma_{21} \frac{\partial u_1}{\partial x_2} + \frac{\partial \sigma_{22}}{\partial x_2} u_2 + \sigma_{22} \frac{\partial u_2}{\partial x_2} + \frac{\partial \sigma_{23}}{\partial x_2} u_3 + \sigma_{23} \frac{\partial u_3}{\partial x_2} +$$

$$\frac{\partial \sigma_{31}}{\partial x_3} u_1 + \sigma_{31} \frac{\partial u_1}{\partial x_3} + \frac{\partial \sigma_{32}}{\partial x_3} u_2 + \sigma_{32} \frac{\partial u_2}{\partial x_3} + \frac{\partial \sigma_{33}}{\partial x_3} u_3 + \sigma_{33} \frac{\partial u_3}{\partial x_3}$$

using tensor notation in the last equation

$$\boldsymbol{\nabla} \cdot (\boldsymbol{\sigma} \cdot \mathbf{u}) = \boldsymbol{\sigma} : (\boldsymbol{\nabla} \otimes \mathbf{u}) + (\boldsymbol{\nabla} \cdot \boldsymbol{\sigma}) \cdot \mathbf{u} \tag{B.6}$$

which is just what it would be expected for the divergence of a product. Notice that $\boldsymbol{\nabla}$, as a differential operator, differentiates both $\boldsymbol{\sigma}$ and $\mathbf{u}$. The substitution of equation (B.6) into (B.2), leads to the final form of the divergence theorem,

$$\int_\Omega \left[\boldsymbol{\sigma} : (\boldsymbol{\nabla} \otimes \mathbf{u}) + (\boldsymbol{\nabla} \cdot \boldsymbol{\sigma}) \cdot \mathbf{u} \right] \mathrm{d}\Omega = \int_\Gamma (\boldsymbol{\sigma} \cdot \mathbf{u}) \cdot \boldsymbol{\nu} \, \mathrm{d}\Gamma \tag{B.7}$$

Here $\boldsymbol{\nabla} \otimes \mathbf{u} = (\partial u_i / \partial x_j)$ is an unsymmetric tensor called the deformation gradient. Considering only its symmetric part $\boldsymbol{\nabla} \otimes \mathbf{u} = \boldsymbol{\nabla}^s \otimes \mathbf{u} = \frac{1}{2}(\boldsymbol{\nabla} \otimes \mathbf{u} + \mathbf{u} \otimes \boldsymbol{\nabla})$, and taking advantage of the symmetry of the stress tensor which implies that $(\boldsymbol{\sigma} \cdot \mathbf{u}) \cdot \boldsymbol{\nu} = (\boldsymbol{\sigma} \cdot \boldsymbol{\nu}) \cdot \mathbf{u}$, the following equation is obtained

$$\int_\Omega \boldsymbol{\sigma} : (\boldsymbol{\nabla}^s \otimes \mathbf{u}) \, \mathrm{d}\Omega = -\int_\Omega (\boldsymbol{\nabla} \cdot \boldsymbol{\sigma}) \cdot \mathbf{u} \, \mathrm{d}\Omega + \int_\Gamma (\boldsymbol{\sigma} \cdot \boldsymbol{\nu}) \cdot \mathbf{u} \, \mathrm{d}\Gamma \tag{B.8}$$

where the outward normal vector $\boldsymbol{\nu}$ to the surface Γ is defined as

$$\boldsymbol{\nu} = \begin{bmatrix} n_1 \\ n_2 \\ n_3 \end{bmatrix} \tag{B.9}$$

Taking the variation of equation B.8 with respect to the displacement field $\mathbf{u}$ while keeping the stress tensor $\boldsymbol{\sigma}$ fixed yields the *Principle of Virtual Work*,

$$\int_\Omega \boldsymbol{\sigma} : (\boldsymbol{\nabla}^s \otimes \boldsymbol{\eta}) \, \mathrm{d}\Omega = -\int_\Omega (\boldsymbol{\nabla} \cdot \boldsymbol{\sigma}) \cdot \boldsymbol{\eta} \, \mathrm{d}\Omega + \int_\Gamma (\boldsymbol{\sigma} \cdot \boldsymbol{\nu}) \cdot \boldsymbol{\eta} \, \mathrm{d}\Gamma \tag{B.10}$$

where $\boldsymbol{\eta} = \delta\mathbf{u}$ is the variation of the displacement field and $\boldsymbol{\nabla}^s \otimes \boldsymbol{\eta} = \delta\boldsymbol{\varepsilon}^u$ is the variation of the strains $\boldsymbol{\varepsilon}^u$ derived from the displacements.

According to the assumptions made in the formulations developed in chapters 4 and 5 where essential boundary conditions are *a priori* satisfied, *i.e.,* $\mathbf{u} = \bar{\mathbf{u}}$, the surface integral of equation B.10 may be simplified, since the variation $\boldsymbol{\eta}$ vanishes on Γ_u, as follows

$$\int_\Omega \boldsymbol{\sigma} : (\boldsymbol{\nabla}^s \otimes \boldsymbol{\eta}) \, \mathrm{d}\Omega = -\int_\Omega (\boldsymbol{\nabla} \cdot \boldsymbol{\sigma}) \cdot \boldsymbol{\eta} \, \mathrm{d}\Omega + \underbrace{\int_{\Gamma_u} (\boldsymbol{\sigma} \cdot \boldsymbol{\nu}) \cdot \boldsymbol{\eta} \, \mathrm{d}\Gamma}_{=0} + \int_{\Gamma_t} (\boldsymbol{\sigma} \cdot \boldsymbol{\nu}) \cdot \boldsymbol{\eta} \, \mathrm{d}\Gamma$$
$$= -\int_\Omega (\boldsymbol{\nabla} \cdot \boldsymbol{\sigma}) \cdot \boldsymbol{\eta} \, \mathrm{d}\Omega + \int_{\Gamma_t} (\boldsymbol{\sigma} \cdot \boldsymbol{\nu}) \cdot \boldsymbol{\eta} \, \mathrm{d}\Gamma \tag{B.11}$$

Note that δ and ∇ are interchangeable: $\nabla\delta u = \delta\nabla u$, *i.e.,* the derivative of the variation is equal to the variation of the derivative [39], a fact used in equation (B.11). This relation is used for the development of the variational formulations of chapters 4 and 5.

To follow a mathematical consistency in the notation employed with the formulations development in this thesis, it is shown that equations B.8 and B.11 may be written in matrix form, and using the Voigt notation for the stress tensor $\boldsymbol{\sigma}$, respectively as

$$\int_\Omega \boldsymbol{\sigma}^T (\mathbf{Du}) \, \mathrm{d}\Omega = -\int_\Omega \left(\boldsymbol{\sigma}^T \mathbf{D}\right) \mathbf{u} \, \mathrm{d}\Omega + \int_{\Gamma_t} \left(\boldsymbol{\sigma}^T \mathbf{P}_\nu\right) \mathbf{u} \, \mathrm{d}\Gamma \tag{B.12}$$

$$\int_\Omega \boldsymbol{\sigma}^T (\mathbf{D}\boldsymbol{\eta}) \, \mathrm{d}\Omega = -\int_\Omega \left(\boldsymbol{\sigma}^T \mathbf{D}\right) \boldsymbol{\eta} \, \mathrm{d}\Omega + \int_{\Gamma_t} \left(\boldsymbol{\sigma}^T \mathbf{P}_\nu\right) \boldsymbol{\eta} \, \mathrm{d}\Gamma \tag{B.13}$$

where the operator $\mathbf{D}$ is called the *symmetric gradient* in the continuum mechanics literature, which in matrix notation is defined as

$$\mathbf{D} = \begin{bmatrix} \frac{\partial}{\partial x_1} & 0 & 0 \\ 0 & \frac{\partial}{\partial x_2} & 0 \\ 0 & 0 & \frac{\partial}{\partial x_3} \\ 0 & \frac{\partial}{\partial x_3} & \frac{\partial}{\partial x_2} \\ \frac{\partial}{\partial x_3} & 0 & \frac{\partial}{\partial x_1} \\ \frac{\partial}{\partial x_2} & \frac{\partial}{\partial x_1} & 0 \end{bmatrix} \tag{B.14}$$

and $\mathbf{P}_\nu$ is the 3×6 normal–projection matrix, which contains the components of the outward normal vector $\mathbf{n}$, given by

$$\mathbf{P}_\nu = \begin{bmatrix} n_1 & 0 & 0 \\ 0 & 0 & n_2 \\ 0 & n_3 & n_2 \\ n_3 & 0 & n_1 \\ n_2 & n_1 & 0 \end{bmatrix} \tag{B.15}$$

Appendix C

Solvability and stability conditions

The use of mixed formulations by means of the finite element method has increased considerably in the last years in almost all fields of science and engineering. This increase in use emerges as a way to obtain reliable and accurate solutions in a wide variety of problems. Mixed finite elements are used in the solution of incompressible fluids flows, irrotational flow of ideal fluids, heat conduction, distribution of electrical or magnetic potentials, torsion or bending of cylindrical beams [22, 23].

The reason why these formulations are not used widely in engineering practice is that their behavior is much more difficult to assess that for the conventional and commonly used displacement formulations. Whereas displacement–based elements, once formulated and shown to work well in certain sets of examples, including the patch test [16, 51, 85, 117, 118], can be generally employed, mixed finite elements cannot be recommended for general use unless a deeper analysis and understanding of the method occurs. A mixed finite element formulation may work properly in the solution of certain problems but perform very poorly on other problems.

Therefore, a mathematical analysis for the solvability and stability of a proposed formulation is an important requirement. Such mathematical analysis should give sufficient insight as to the general applicability of the formulations under consideration and is, in general, not an easy task [16, 20, 22, 23, 107].

This mathematical theory is commonly referred in literature as the Babuška–Brezzi condition [12, 23, 117, 118], LBB condition [11, 12, 33], or inf–sup condition [12, 16, 17, 22, 23, 107]. In this work, this condition is referred as the Babuška–Brezzi condition (BB).

The BB condition uniform is accepted as a necessary condition for a robust finite element formulation. In this section a simple way in the presentation of the BB is developed for its implementation in a practical algorithm; for a more detailed study of the BB condition, the reader is referred to [11, 12, 16, 17, 20, 22, 23, 33]

Implementation of mixed variational formulations, developed in chapter 4, with the finite element method leads to linear algebraic systems of the general form

$$\begin{bmatrix} \mathbf{A} & \mathbf{B}^{\mathrm{T}} \\ \mathbf{B} & \mathbf{0} \end{bmatrix} \begin{Bmatrix} \mathbf{x} \\ \mathbf{y} \end{Bmatrix} = \begin{Bmatrix} \mathbf{f} \\ \mathbf{g} \end{Bmatrix} \tag{C.1}$$

where $\mathbf{A}$ and $\mathbf{B}$ are matrices of dimensions $n \times n$ and $m \times n$ respectively, while $\mathbf{x}$ and $\mathbf{y}$ are vectors of $n \times 1$ and $m \times 1$ dimensions respectively, as well as $\mathbf{f}$ and $\mathbf{g}$. In the next section a simple algebraic version, of the abstract theory of the the solvability and stability related with mixed finite element formulations is presented.

C.1 Solvability condition

Within the context of solution of systems of equations, solvability means that for every right–hand side $\mathbf{f}$ and $\mathbf{g}$, the system (C.1) has a unique solution [107]. It is well known that this property holds, if and only if, the $(n + m) \times (n + m)$ matrix

$$\begin{bmatrix} \mathbf{A} & \mathbf{B}^{\mathrm{T}} \\ \mathbf{B} & \mathbf{0} \end{bmatrix} \tag{C.2}$$

is *nonsingular*, that is, if and only if, its determinant is different from zero. Another way to express solvability of the system (C.1) is that the homogeneous system

$$\begin{bmatrix} \mathbf{A} & \mathbf{B}^{\mathrm{T}} \\ \mathbf{B} & \mathbf{0} \end{bmatrix} \begin{Bmatrix} \mathbf{x} \\ \mathbf{y} \end{Bmatrix} = \begin{Bmatrix} \mathbf{0} \\ \mathbf{0} \end{Bmatrix} \tag{C.3}$$

has only for solution the trivial:

$$\begin{Bmatrix} \mathbf{x} \\ \mathbf{y} \end{Bmatrix} = \begin{Bmatrix} \mathbf{0} \\ \mathbf{0} \end{Bmatrix} \tag{C.4}$$

This is another way to say that the homogeneous system (C.3) has only the trivial solution (C.4), which implies that the determinant of the matrix (C.1) is different from zero, and hence the system is solvable.

C.2 Stability condition

The other important condition necessary to have an stable method, is to guarantee the convergence in its numerical implementation. Systems like (C.1) have to satisfy some

conditions; specifically matrices **A** and **B**, defined in equation C.2. For the purpose of this thesis, the discussion will focus only in the BB condition which is directly related with matrix **B**; while conditions for matrix **A** are out of the scope of this study since, they are verified in practice only for the Stokes problem [107].

The BB condition requires the existence of a positive constant β, independent of the mesh size h, such that:

$$\mathbf{x}^{\mathrm{T}}\mathbf{B}^{\mathrm{T}}\mathbf{y} \geq \beta \left\| \mathbf{x} \right\|_X \left\| \mathbf{y} \right\|_Y \tag{C.5}$$

Condition (C.5) has to be hold for all $\mathbf{y} \in \mathbf{Y}$ such that a suitable $\mathbf{x} \in \mathbf{X}$, different from $\mathbf{0}$ can be found.

Stability of the mixed method is hold if matrix **B** is *injective* [107]; this implies that the number of equations n has to be at least equal or greater than the number of equations m:

$$n \geq m \tag{C.6}$$

For the strain–displacement formulation, developed in section 5.2.2; the BB condition requires that the number of strain degrees of freedom has to be at least equal or greater than the number of displacement degrees of freedom.

Bibliography

[1] J. Alfaiate. Strong discontinuities embedded in finite elements. Technical Report Relatório ICIST, DTC no. 09/00, Instituto Superior Técnico, Lisbon, Portugal, 2000.

[2] J. Alfaiate, E. B. Pires, and J. A. C. Martins. A finite element analysis of non–prescribed crack propagation in concrete. *Computers and Structures*, 63(1):17–26, 1997.

[3] J. Alfaiate, A. Simone, and L. J. Sluys. Non–homogeneous displacement jumps in strong embedded discontinuities. *International Journal of Solids and Structures*, 40:5799–5817, 2003.

[4] J. Alfaiate, G. N. Wells, and L. J. Sluys. On the use of embedded discontinuity elements with crack path continuity for mode–I and mixed–mode fracture. *Engineering Fracture Mechanics*, 69(6):661–686, 2002.

[5] E. Anderson, Z. Bai, C. Bischof, S. Blackford, J. Demmel, J. Dongarra, J. Du Croz, A. Greenbaum, S. Hammarling, A. Mckenney, and D. Sorensen. *LAPACK. Users' Guide*. SIAM, Philadelphia, 1999.

[6] T. L. Anderson. *Fracture Mechanics*. CRC Press, Boca Raton, 1995.

[7] G. B. Arfken and H. J. Weber. *Mathematical Methods for Physicists*. Elsevier Academic–Press, New York, 2005.

[8] F. Armero and K. Garikipati. An analysis of strong discontinuities in multiplicative finite strain plasticity and their relation with the numerical simulation of strain localization in solids. *International Journal of Solids and Structures*, 33(20–22):2863–2885, 1996.

[9] F. Armero and C. Linder. New finite elements with embedded strong discontinuities in the finite deformation range. *Computer Methods in Applied Mechanics and Engineering*, 197:3138–3170, 2008.

[10] M. Arrea and A. Ingraffea. Mixed mode crack propagation in mortar and concrete. Technical Report 81–13, Dpt. of Structural Engineering, Cornell University, Ithaca, New York, 1982.

[11] F. Auteri, J. L. Guermond, and N. Parolini. Role of the LBB condition in weak spectral projection methods. *Journal of Computational Physics*, 174(1):405–420, 2001.

[12] I. Babuška and R. Narasimhan. The Babuška–Brezzi condition and the patch test: an example. *Computer Methods in Applied Mechanics and Engineering*, 140(1–2):183–199, 1997.

[13] Z. P. Bažant. Why continuum damage is nonlocal: Micromechanics arguments. *Journal of Engineering Mechanics*, 117:1070–1087, 1991.

[14] Z. P. Bažant and J. Planas. *Fracture and Size Effect in Concrete and Other Quasibrittle Materials*. CRC Press, Boca Raton, 1998.

[15] G. I. Barenblatt. The mathematical theory of equilibrium of cracks in brittle fracture. *Archive of Applied Mechanics*, 7:55–129, 1962.

[16] K. Bathe. *Finite Element Procedures in Engineering Analysis*. Prentice–Hall, Englewood Cliffs, New Jersey, 1996.

[17] K. J. Bathe, D. Hendriana, F. Brezzi, and G. Sangalli. Inf–sup testing of upwind methods. *International Journal for Numerical Methods in Engineering*, 48(5):745–760, 2000.

[18] T. Belytschko, J. Fish, and B. Engelmann. A finite element with embedded localization zones. *Computer Methods in Applied Mechanics and Engineering*, 70:59–89, 1988.

[19] T. Belytschko, W. K. Liu, and B. Moran. *Nonlinear Finite Elements for Continua and Structures*. John Wiley, Chichester, 2006.

[20] D. Boffi, F. Brazzi, L. F. Demkowicz, R. G. Durán, R. S. Falk, and M. Fortin. *Mixed Hybrid Finite Elements, Compatibility Conditions, and Applications*. Springer–Verlag, Cetraro, Italy, 2006.

[21] R. Borst. Numerical aspects of cohesive–zone models. *Engineering Fracture Mechanics*, 70:1743–1757, 2003.

[22] F. Brezzi and K. J. Bathe. A discourse on the stability conditions for mixed finite element formulations. *Computer Methods in Applied Mechanics and Engineering*, 82:27–57, 1990.

[23] F. Brezzi and M. Fortin. *Mixed and Hybrid Finite Element Methods*. Springer–Verlag, New York, 1991.

[24] K. B. Broberg. *Cracks and Fracture*. Academic Press, London, 1999.

[25] W. F. Carroll. *A primer for Finite Elements in Elastic Structures*. John Wiley, New York, 1999.

[26] E. W. V Chaves. *A three Dimensional Setting for Strong Discontinuities Modelling in Failure Mechanics*. PhD thesis, Universitat Politécnica de Catalunya, Barcelona, 2003.

[27] D. Dias da Costa, J. Alfaiate, L. J. Sluys, and E. Júlio. A discrete strong discontinuity approach. *Engineering Fracture Mechanics*, 76:1176–1201, 2009.

[28] D. Dias da Costa, J. Alfaiate, L. J. Sluys, and E. Júlio. Towards a generalization of a discrete strong discontinuity approach. *Computer Methods in Applied Mechanics and Engineering*, 198:3670–3681, 2009.

[29] R. de Borst, M. A. Gutiérrez, G. N. Wells, J. J. C. Remmers, and H. Askes. Cohesive–zone models, higher–order continuum theories and reliability methods for computational failure analysis. *International Journal for Numerical Methods in Engineering*, 60:289–315, 2004.

[30] B. Fraeijs de Veubeke. Diffusion des inconnues hyperstatiques dans les voilures à longeron couplés. Technical Report 24, Bull. Serv. Tecnhique de L'Aéronautique, Brussels, 1951.

[31] B. Fraeijs de Veubeke. Displacement and equilibrium models in the finite element method. *International Journal for Numerical Methods in Engineering*, 52:287–342, 2001. Classical reprint series.

[32] P. Deuflhard. *Newton Methods for Nonlinear Problems*. Springer–Verlag, Berlin Heidelberg, 2004.

[33] M. Dobrowolski. On the LBB condition in the numerical analysis of the Stokes equations. *Applied Numerical Mathematics*, 54(3–4):314–323, 2004.

[34] J. E. Dolbow. *An extended Finite Element Method with Discontinuous Enrichment for Applied Mechanics*. PhD thesis, Northwestern University, Evanston, Illinois, 1999.

[35] J. J. Dongarra, C. B. Moler, J. R. Bunch, and G. W. Stewart. *LINPACK. Users' Guide*. SIAM, Philadelphia, 1979.

[36] D. S. Dugdale. Yielding of steel sheets containing slits. *Journal of the Mechanics and Physics of Solids*, 8:100–104, 1960.

[37] E. N. Dvorkin. Finite elements with displacement interpolated embedded localization lines insensitive to mesh size and distortions. *International Journal for Numerical Methods in Engineering*, 30:541–564, 1990.

[38] M. Elices, G. V. Guinea, J. Gómez, and J. Planas. The cohesive zone model: advantages, limitations and challenges. *Engineering Fracture Mechanics*, 69:137–163, 2002.

[39] L. Elsgolts. *Differential Equations and the Calculus of Variations.* Mir publishers, Moscow, 1970.

[40] C. A. Felippa. Web–posted Lectures on Advanced Finite Element Methods, at http://caswww.colorado.edu/courses.d/AFEM.d/home.html. Updated each Fall semester.

[41] L. Fernández. *Modelado Numérico de la Fractura en el Concreto.* PhD thesis, Universidad Nacional Autónoma de México, Mexico, 2002.

[42] L. E. Fernández and G. Ayala. Constitutive modeling of discontinuities by means of discrete and continuum approximations and damage models. *International Journal of Solids and Structures*, 41:1453–1471, 2004.

[43] Y. C. Fung. *Foundations of Solid Mechanics.* Prentice–Hall, New Jersey, 1965.

[44] G. Pijaudier-Cabot G. and Z. P. Bažant. Nonlocal damage theory. *Journal of Engineering Mechanics, ASCE*, 37:1512–1533, 1987.

[45] M. G. D. Geers. Continuum damage mechanics. Technical Report Lecture notes – course 4K060, Materials Technology, Mechanical Engineering, Eindhoven University of Technology, Eindhoven, The Netherlands, 1999.

[46] P. Germain, Q. S. Nguyen, and P. Suquet. Continuum thermodynamics. *Transactions of the ASME*, 50:1010–1020, 1983.

[47] G. H. Golub and C. F. Van Loan. *Matrix Computations.* The Johns Hopkins University Press, Baltimore, Maryland, 1996.

[48] D. Hegen. *An Element–Free Galerkin Method for Crack Propagation in Brittle Materials.* PhD thesis, Eindhoven University of Technology, Eindhoven, The Netherlands, 1997.

[49] A. Hillerborg, M. Modeer, and P. E. Petersson. Analysis of crack formation and crack growth in concrete by means of fracture mechanics and finite elements. *Cement and Concrete Research*, 6:773–782, 1976.

[50] G. A. Holzapfel. *Nonlinear Solid Mechanics.* John Wiley, New York, 2000.

[51] T. J. R. Hughes. *The Finite Element Method.* Prentice–Hall, Englewood Cliffs, New Jersey, 1987.

[52] C. E. Inglis. Stress in a plate due to the presence of crack and sharp corners. *Transactions of the Institution of Naval Architects*, 55:219–241, 1913.

[53] M. Jirásek. Numerical modeling of deformation and failure materials, lecture notes. Department of Mechanics, Faculty of Civil Engineering, Czech Technical University in Prague, Czech Republic, 2000.

[54] M. Jirásek. Finite elements with embedded cracks. Technical Report LSC Internal Report 98/01, École Polytechnique Fédérale de Lausanne, Lausanne, Switzerland, 1998.

[55] M. Jirásek. Comparative study on finite elements with embedded discontinuities. *Computer Methods in Applied Mechanics and Engineering*, 188:307–330, 2000.

[56] M. Jirásek and B. Patzák. Consistent tangent stiffness for nonlocal damage models. *Computers and Structures*, 80:1279–1293, 2002.

[57] M. Jirásek and S. Rolshoven. Comparison of integral–type nonlocal plasticity models for strain–softening materials. *International Journal of Engineering Science*, 41:1553–1602, 2003.

[58] M. Jirázek and Z. P. Bažant. *Inelastic Analysis of Structures.* John Wiley, Chichester, 2002.

[59] G. Juárez. *Modelado Numérico de Problemas de Fractura en Sólidos Mediante Discontinuidades Interiores.* PhD thesis, Universidad Nacional Autónoma de México, Mexico, 2006.

[60] G. Juárez and A. G. Ayala. Variational formulation of the material failure process in solids by embedded discontinuities model. *Numerical Methods for Partial Differential Equations*, 25:26–62, 2009.

[61] L. M. Kachanov. Time of the rupture process under creep conditions. *Isv. Akad. Nauk SSSR, Otd. Tehk. Nauk*, 8:26–31, 1958.

[62] C. T. Kelley. *Solving Nonlinear Equations with Newton's Method.* SIAM, Philadelphia, 2003.

[63] N. Kikuchi. *Finite Element Methods in Mechanics.* Cambridge University Press, London, 1986.

[64] R. Larsson and K. Runesson. Element–embedded localization band based on regularized displacement discontinuity. *ASCE Journal of Engineering Mechanics*, 122(5):402–411, 1996.

[65] J. Lemaitre. *A Course on Damage Mechanics.* Springer–Verlag, Berlin Heidelberg, 1996.

[66] J. Lemaitre and R. Desmorat. *Engineering Damage Mechanics.* Springer–Verlag, Berlin Heidelberg, 2005.

[67] Y. N. Li and Z. P. Bažant. Eigenvalue analysis of size effect for cohesive crack model. *International Journal of Fracture*, 66:213–226, 1994.

[68] C. Linder and F. Armero. Finite elements with embedded branching. *Finite Elements in Analysis and Design*, 45:280–293, 2009.

[69] H. R. Lotfi and P. B. Shing. Embedded representation of fracture in concrete with mixed finite elements. *International Journal for Numerical Methods in Engineering*, 38:1307–1325, 1995.

[70] B. Luccioni, S. Oller, and R. Danesi. Coupled plastic–damaged model. *Computer Methods in Applied Mechanics and Engineering*, 129:81–89, 1996.

[71] L. E. Malvern. *Introduction to the Mechanics of a Continuous Medium.* Prentice–Hall, Englewood Cliffs, New Jersey, 1969.

[72] C. D. Meyer. *Matrix Analysis and Applied Linear Algebra.* SIAM, Philadelphia, 2000.

[73] S. Mohammadi. *Extended Finite Element Methods.* Blackwell Publishing, Oxford, 2008.

[74] J. Mosler. On the modeling of highly localized deformations induced by materials failure: The strong discontinuity approach. *Archives of Computational Methods in Engineering*, 11:389–446, 2004.

[75] J. Mosler. A novel algorithmic framework for the numerical implementation of locally embedded strong discontinuities. *Computer Methods in Applied Mechanics and Engineering*, 194:4731–4757, 2005.

[76] A. Mota and J. F. Abel. On mixed finite element formulations and stress recovery techniques. *International Journal for Numerical Methods in Engineering*, 47:191–204, 2000.

[77] A. A. Mota. *A Class of Geometrically Exact Membrane and Cable Finite Elements Based on the Hu–Washizu Functional.* PhD thesis, Cornell University, Ithaca, New York, 2000.

[78] J. Oliver. Modelling strong discontinuities in solid mechanics via strain softening constitutive equations. Part 1: Fundamentals. *International Journal for Numerical Methods in Engineering*, 39(21):3575–3600, 1996.

[79] J. Oliver. Modelling strong discontinuities in solid mechanics via strain softening constitutive equations. Part 2: Numerical simulation. *International Journal for Numerical Methods in Engineering*, 39(21):3601–3623, 1996.

[80] J. Oliver and A. E. Huespe. Theoretical and computational issues in modelling material failure in strong discontinuity scenarios. *Computer Methods in Applied Mechanics and Engineering*, 193:2987–3014, 2004.

[81] J. Oliver, A. E. Huespe, and P. J. Sánchez. A comparative study on finite elements for capturing strong discontinuities: E–FEM vs X–FEM. *Computer Methods in Applied Mechanics and Engineering*, 195:4732–4752, 2006.

[82] S. Oller. *Fractura mecánica. Un enfoque global.* Ediciones UPC, Barcelona, 2001.

[83] J. K. Pamin. *Gradient–Dependent Plasticity in Numerical Simulation of Localization Phenomena.* PhD thesis, Delft University of Technology, Delft, The Netherlands, 1993.

[84] T. Rabczuk and T. Belytschko. Adaptivity for structured meshfree particle method in 2D and 3D. *International Journal for Numerical Methods in Engineering*, 63:1559–1582, 2005.

[85] J. N. Reddy. *A Introduction to the Finite Element Method.* McGraw–Hill, New York, 1993.

[86] J. Retama and G. Ayala. Modelado de la propagación de grietas en sólidos mediante formulaciones variacionales de discontinuidades interiores y elementos finitos mixtos. in: CIMN 2010, V Congreso Internacional de Métodos Numéricos, Guanajuato, Mexico, 2010.

[87] J. Retama and G. Ayala. Modelado del daño en sólidos mediante formulaciones variacionales de discontinuidades interiores. *Rev. Int. Mét. Num. Cálc. Dis. Ing.*, accepted for publication.

[88] J. Retama and G. Ayala. Modeling of damage in solids by weak and discrete embedded discontinuities approximations. in: USNCCM 2009, 10th. US National Congress on Computational Mechanics, Columbus, Ohio, 2009.

[89] J. Retama and G. Ayala. Modelling of failure in solids by embedded discontinuities. Displacements and strain–displacements formulations of finite element. in: WCCM 2008, 8th. World Congress on Computational Mechanics, Venice, Italy, 2008.

[90] J. Retama, G. Ayala, M. Cuomo, and L. Contrafatto. Consistent symmetric formulation of the enhanced embedded discontinuity method. in: ECCM 2010, IV European Conference on Computational Mechanics, Paris, 2010.

[91] J. Retama, G. Ayala, and G. Juárez. A comparative study of a hierarchy of finite elements formulations with embedded discontinuities. in: USNCCM 2007, 9th. US National Congress on Computational Mechanics, San Francisco CA, 2007.

[92] J. Retama, G. Juárez, and G. Ayala. Aplicación de la mecánica del daño a la solución de problemas de Ingeniería estructural. in: SMIE 2008, XVI Congreso Nacional de Ingeniería Estructural, Veracrúz, Mexico, 2008.

[93] J. G. Rots. *Computational Modeling of Concrete Fracture.* PhD thesis, Delft University of Technology, Delft, The Netherlands, 1988.

[94] E. Samaniego. *Contributions to the Continuum Modelling of Strong Discontinuities in Two–Dimensional Solids.* PhD thesis, Universitat Politécnica de Catalunya, Barcelona, 2003.

[95] J. M. Sancho, J. Planas, D. A. Cendón, E. Reyes, and J. C. Gálvez. En embedded crack model for finite element analysis of concrete fracture. *Engineering Fracture Mechanics*, 74:75–86, 2007.

[96] V. E. Saouma. Advanced mechanics of materials, lecture notes. Department of Civil Environmental and Architectural Engineering, University of Colorado, Boulder, 2002.

[97] E. Schlangen. Experimental and numerical analysis of fracture processes in concrete. *HERON*, 38(2), 1993.

[98] E. Schlangen. *Experimental and Numerical Analysis of Fracture Processes in Concrete*. PhD thesis, Delft University of Technology, Delft, The Netherlands, 1993.

[99] J. C. Simo and T. J. R. Hughes. On the variational foundations of assumed strain methods. *ASME J. of Appl. Mech.*, 53:51–54, 1986.

[100] J. C. Simo and T. J. R. Hughes. *Computational Inelasticity*. Springer–Verlag, New York, 1998.

[101] J. C. Simo, J. Oliver, and F. Armero. An analysis of strong discontinuities induced by strain–softening in rate–independent inelastic solids. *Computational Mechanics*, 12:277–296, 1993.

[102] J. C. Simo and M. S. Rifai. A class of mixed assumed strain methods and the method of incompatible modes. *International Journal for Numerical Methods in Engineering*, 29(8):1595–1638, 1990.

[103] A. Simone. *Continuous–Discontinuous Modelling of Failure*. PhD thesis, Delft University of Technology, Delft, The Netherlands, 2003.

[104] A. Simone, J. J. C. Remmers, and G. N. Wells. An interface element based on the partition of unity. Technical Report CM2001.007, Delft University of Technology, Delft, The Netherlands, 2000.

[105] J. W. Simons and G. H. Powell. Solution strategies for statically loaded nonlinear structures. Technical Report No. UCB/EERC–82/22, Earthquake Engineering Research Center, University of California, Berkeley, 1982.

[106] S. H. Song. *Fracture of Asphalt concrete: A Cohesive Zone Modeling Approach Considering Viscoelastic Effects*. PhD thesis, University of Illinois, Champaign, Urbana, 2006.

[107] E. Stein, R. De Borst, and T. J. R. Hughes. *Encyclopedia of Computational Mechanics. Volume 1: Fundamentals*, chapter 9. John Wiley, New York, 2004.

[108] R. L. Taylor. FEAP: A Finite Element Analysis Program. Department of Civil and Environmental Engineering, University of California, Berkeley.

[109] R. L. Taylor. FEAP: A Finite Element Analysis Program, theory manual. Department of Civil and Environmental Engineering, University of California, Berkeley, 2008.

[110] M. G. A. Tijssens. *On the Cohesive Surface Methodology for Fracture of Brittle Heterogeneous Solids.* PhD thesis, Delft University of Technology, Delft, The Netherlands, 2000.

[111] M. R. A. Van Vliet. *Size Effect in Tensile Fracture of Concrete and Rock.* PhD thesis, Delft University of Technology, Delft, The Netherlands, 2000.

[112] G. Z. Voyiadjis and P. I. Kattan. *Damage Mechanics.* CRC Press, Boca Raton, 2005.

[113] K. Washizu. *Variational Methods in Elasticity and Plasticity.* Pergamon Press, Oxford, 1982.

[114] G. N. Wells. *Discontinuous Modelling of Strain Localization and Failure.* PhD thesis, Delft University of Technology, Delft, The Netherlands, 2001.

[115] G. N. Wells and L. J. Sluys. A new method for modelling cohesive cracks using finite elements. *International Journal for Numerical Methods in Engineering*, 50:2667–2682, 2001.

[116] G. N. Wells and L. J. Sluys. Three–dimensional embedded discontinuity model for brittle fracture. *International Journal of Solids and Structures*, 38(5):897–913, 2001.

[117] O. C. Zienkiewicz and R. L. Taylor. *The Finite Element Method. Volume 1: The Basis.* Butterworth–Heinemann, Oxford, 2000.

[118] O. C. Zienkiewicz, R. L. Taylor, and J. Z. Zhu. *The Finite Element Method. Volume 1: Its Basis and fundamentals.* Butterworth–Heinemann, Oxford, 2005.

[119] O. C. Zienkiewicz and J. Z. Zhu. The superconvergent patch recovery and a posteriori error estimates. Part 1: The recovery techniques. *International Journal for Numerical Methods in Engineering*, 33:1331–1364, 1992.

Acknowledgements

Firstly I would like to express my most sincere thanks to Professor A. Gustavo Ayala Milián by sharing his knowledge with me and for his advice in the development of this thesis.

I am very grateful to Professor J. Alfaiate for his support during my academic stay at the *Instituto Superior Técnico* of Lisbon Portugal (**IST**). Equally I greatly appreciate to Professors L. Contrafatto and M. Cuomo of the *Università degli Studi di Catania* in Italy (**UNICT**) by their advice and suggestions in the development of this research work.

<div align="right">

Jaime Retama Velasco
Mexico D.F., Mexico
September 2010

</div>